Climatological Analysis of Tropical Cyclone Intensity Changes under Moderate Vertical Wind Shear

ROSIMAR RIOS-BERRIOS AND RYAN D. TORN

Department of Atmospheric and Environmental Sciences, University at Albany, State University of New York, Albany, New York

(Manuscript received 9 September 2016, in final form 20 December 2016)

ABSTRACT

Although infrequent, tropical cyclones (TCs) can intensify under moderate vertical wind shear (VWS). A potential hypothesis is that other factors—associated with both the TC and its environment—can help offset the effects of VWS and aid intensification. This hypothesis was tested with a large dataset of 6-hourly best tracks and environmental diagnostics for global TCs between 1982 and 2014. Moderate VWS was objectively defined as 4.5–11.0 m s^{-1}, which represents the 25th–75th percentiles of the global distribution of 200–850-hPa VWS magnitude around TCs. Intensifying events (i.e., unique 6-hourly data points) were compared against steady-state events to determine which TC and environmental characteristics favored intensification under moderate VWS. This comparison showed that intensifying events were significantly stronger, closer to the equator, larger, and moving with a more westward motion than steady-state events. Furthermore, intensifying events moved within environments characterized by warmer sea surface temperatures, greater midtropospheric water vapor, and more easterly VWS than steady-state events. Storm-relative, shear-relative composites suggested that the coupling between water vapor, surface latent heat fluxes, and storm-relative flow asymmetries was conducive for less dry air intrusions and more symmetric rainfall in intensifying events. Last, the comparison showed no systematic differences between environmental wind profiles possibly due to the large temporal variability of VWS.

1. Introduction

Environmental vertical wind shear (VWS) is one of the most inhibiting factors for tropical cyclone (TC) intensification. Climatological analyses for TCs in different basins consistently show that the stronger the VWS, the smaller the chances of intensification (Merrill 1988; DeMaria and Kaplan 1994; Kaplan and DeMaria 2003; Paterson et al. 2005; Hendricks et al. 2010). The importance of VWS is also evident in statistical–dynamical intensity prediction models, which typically rank VWS as one of the top environmental predictors of TC intensity changes (e.g., DeMaria and Kaplan 1999; Emanuel et al. 2004). However, the likelihood and timing of intensification becomes highly uncertain under moderate VWS (Zhang and Tao 2013; Tao and Zhang 2015), which can be defined as the range of VWS magnitudes that are neither too weak to have little influence on intensity changes nor too strong to completely halt intensification. Intensity forecasts for TCs under moderate VWS are characterized by large errors (Bhatia and Nolan 2013), presumably because other factors—associated with both the TC and its environment—can help offset the negative effects of VWS and lead to intensification. A comprehensive analysis is needed to identify TC and environmental characteristics that are conducive for intensification under moderate VWS.

Certain kinematic aspects of the TC vortex, such as size, intensity, and latitude, can impact intensity changes in sheared environments (Jones 1995; DeMaria 1996; Reasor et al. 2004; Riemer and Montgomery 2011; Tang and Emanuel 2012; Riemer et al. 2013; Reasor and Montgomery 2015). Given that VWS tilts the vortex from its upright position, vortex realignment is a process by which a TC can overcome the effects of VWS and intensify in a sheared environment. Various mechanisms have been proposed to explain vortex realignment, including vortex precession (Jones 1995) and damping of vortex Rossby waves (Reasor et al. 2004). Regardless of the physical mechanism, theoretical and idealized

Corresponding author e-mail: Rosimar Rios-Berrios, rrios-berrios@albany.edu

DOI: 10.1175/MWR-D-16-0350.1

modeling studies agree that large, strong, and high-latitude TCs have faster vortex realignment than small, weak, low-latitude TCs (Jones 1995; DeMaria 1996; Reasor et al. 2004; Reasor and Montgomery 2015). The size and intensity of a TC circulation can also modulate the resilience of a TC to another effect of VWS—dry air intrusion. Large and strong TCs in numerical simulations are less prone to dry air intrusions than small and weak TCs (Riemer and Montgomery 2011; Riemer et al. 2013). Furthermore, the effects of dry air intrusion on intensity change depend on the initial intensity, such that the same amount of dry intrusion could be more detrimental for a weak TC than for a strong TC (Tang and Emanuel 2010, 2012). The applicability of these results to observed TCs under moderate VWS remains unknown.

Kinematic aspects of the TC environment, such as the shape of the environmental wind profile, could also influence intensity changes in sheared environments (Zeng et al. 2010; Onderlinde and Nolan 2014, 2016; Wang et al. 2015; Finocchio et al. 2016). Through idealized simulations and a statistical analysis, Onderlinde and Nolan (2014) showed that development and intensification happens faster when the environmental winds rotate clockwise with height [i.e., positive tropical cyclone–relative helicity (TCREH)] compared to when the environmental winds rotate counterclockwise with height (negative TCREH). Intensification happens faster under positive TCREH because surface latent heat fluxes are stronger cyclonically upwind of the shear-organized convection, and this setup aids the azimuthal propagation of convection and vortex realignment (Onderlinde and Nolan 2016). Using the same modeling framework as in Onderlinde and Nolan (2014), Finocchio et al. (2016) tested the sensitivity of intensity changes to the height and depth of VWS. Their simulations showed that intensification happens faster in environments where the shear is concentrated in the upper troposphere than in environments where the shear is concentrated in the lower troposphere. Finocchio et al. (2016) attributed the different intensification rates to the timing and likelihood of vortex realignment. A potential limitation of these studies is that VWS was held constant throughout five days, which may not be a good representation of real environments. Nevertheless, recent statistical studies have also found sensitivity of intensity change to the layer of VWS (Zeng et al. 2010; Wang et al. 2015).

Thermodynamic characteristics of the TC and the environment can also be influential for intensification under moderate VWS (Molinari et al. 2004, 2006; Shelton and Molinari 2009; Nguyen and Molinari 2012; Reasor and Eastin 2012; Chen and Gopalakrishnan 2015; Nguyen and Molinari 2015). Persistent convective outbreaks in the downshear quadrant and inside the radius of maximum winds were linked to the intensification of Hurricane Danny (1997; Molinari et al. 2004), Hurricane Irene (1999; Nguyen and Molinari 2012), Tropical Storm Gabrielle (2001; Molinari et al. 2006; Nguyen and Molinari 2015), and Hurricane Claudette (2003; Shelton and Molinari 2009). These convective outbreaks happened when the TCs moved over warm sea surface temperatures (SST) of at least 28°C and through near-saturated environments. In the case of Hurricane Claudette, convective activity ceased and the TC weakened shortly after dry air from the upshear quadrant was mixed into the eyewall. Similarly, Molinari et al. (2013) noted that Tropical Storm Edouard (2002)—despite having intense downshear convection—did not intensify, possibly because convection was far removed from the TC center and the upshear semicircle was remarkably dry. These findings hint that environmental thermodynamic characteristics, such as SST and upshear moisture, can modulate convective outbreaks and intensity changes under moderate VWS.

Recent modeling studies agree that SST and environmental moisture modulate the likelihood of intensification under moderate VWS (Ge et al. 2013; Munsell et al. 2013; Tao and Zhang 2014; Rios-Berrios et al. 2016a,b). Increasing the SST from 27° to 29°C increased the chances of intensification under VWS as large as 12.5 $m\,s^{-1}$ in the idealized simulations of Tao and Zhang (2014). The increased chances of intensification were attributed to enhanced surface latent heat fluxes leading to more vigorous convection and faster vortex realignment. Rios-Berrios et al. (2016a,b) demonstrated the influence of environmental moisture in ensemble intensity forecasts of Hurricanes Katia (2011) and Ophelia (2011). Significant differences in *lower*-tropospheric moisture *right* of the shear vector led to differences among ensemble intensity forecasts of Katia (Rios-Berrios et al. 2016a), whereas significant differences in *middle* tropospheric moisture *left* of the shear vector led to differences among ensemble intensity forecasts of Ophelia (Rios-Berrios et al. 2016b). In both cases, enhanced moisture led to intensification through a combination of vortex stretching in the lower troposphere and tilting of horizontal vorticity in the middle troposphere. Discrepancies in the location of enhanced moisture between the two cases demand further investigation with a larger sample size.

A climatological analysis could potentially provide more information about TC intensity changes under moderate VWS by considering multiple cases. Previous climatological studies, however, have been limited to either correlation analyses with a relatively small sample

size (DeMaria 1996), composites of airborne Doppler observations of predominantly major Atlantic hurricanes (Rogers et al. 2013), or statistical analyses based on individual basins (Zeng et al. 2010; Wang et al. 2015). This study addresses those limitations by performing a comprehensive climatological analysis based on multiple cases from multiple basins. A combined dataset of best tracks and environmental diagnostics was created to consider all TCs around the world between 1982 and 2014. Data sources and restrictions applied to the database are discussed in section 2. The database was used to identify TCs with different intensity changes, objectively define moderate VWS, and to perform a statistical comparison of TCs that either did or did not intensify under moderate VWS. Results from this comparison are discussed in section 3, followed by conclusions and suggestions for future work in section 4.

2. Approach

a. Datasets

1) Best tracks

The International Best Track Archive for Climate Stewardship (IBTrACS; Knapp et al. 2010) dataset was used to gather information about TCs around the world. IBTrACS combines best tracks from all operational centers in individual files that are consistently formatted for all basins. In this study, the IBTrACS-all dataset was used to obtain best tracks from the National Hurricane Center (NHC) for North Atlantic and eastern North Pacific TCs, and from the Joint Typhoon Warning Center (JTWC) for western North Pacific, South Pacific, and Indian Ocean TCs. The location of each TC was identified using the latitude, longitude, and distance from land variables from IBTrACS. TC intensity was measured by the maximum sustained wind speed. Additional quantities were derived from the aforementioned variables, including TC intensity change (temporal change of maximum sustained wind speed) and TC translational speed (determined from a 12-h centered finite difference in TC position).

2) Reanalysis datasets

The atmospheric state surrounding TCs was evaluated using reanalysis datasets. This choice was made because direct observations over the tropical oceans are sparse; however, a reanalysis should be considered as an approximation rather than a true representation of the atmosphere. Two different reanalysis datasets were used to verify the robustness of the climatological analysis: the European Centre for Medium-Range Weather Forecasts (ECMWF) interim reanalysis (ERA-Interim, hereafter ERAI) dataset (ECMWF 2009; Dee et al. 2011), and the National Centers for Environmental Prediction (NCEP) Climate Forecast System Reanalysis (CFSR), version 2 dataset (Saha et al. 2010, 2014). Results based on both datasets were consistent; therefore, only ERAI results are presented here.

The ERAI is produced with the ECMWF Integrated Forecast System, which consists of three fully-coupled components for the atmosphere, land surface, and ocean waves (Dee et al. 2011). Multiple observations are combined with short-term forecasts using a four-dimensional variational data assimilation system. The 6-hourly analyses are produced on a gridded domain with approximately 79-km horizontal grid spacing and 60 vertical levels extending up to 0.1 hPa. This study considered 6-hourly analyses between 1982 and 2014 for consistency with the IBTrACS and SST datasets. Because of the large number of cases considered and extensive calculations performed, interpolated analyses were obtained from the Research Data Archive (RDA) via the National Center for Atmospheric Research (NCAR) Yellowstone computing system (Computational and Information Systems Laboratory 2012). Interpolated fields were available on a 0.703° × 0.702° latitude–longitude Gaussian grid on isobaric surfaces.

3) SST analyses

SST information near each TC center was obtained from the National Oceanic and Atmospheric Administration (NOAA) optimum interpolation (OI) SST version 2 dataset (Reynolds et al. 2002). This dataset—produced by NOAA's National Climatic Data Center (now National Centers for Environmental Information)—provides different analysis products that combine in situ ocean observations (e.g., from buoys, ships, etc.) with infrared satellite measurements. The specific product used here provided daily SST analyses on a 0.25° × 0.25° latitude–longitude grid (NCDC/NESDIS/NOAA 2007; Reynolds et al. 2007; Banzon and Reynolds 2013). This dataset was also accessed through the RDA.

4) Precipitation rates

Precipitation rates were evaluated as proxies for rainfall associated with the TCs. The Tropical Rainfall Measuring Mission (TRMM) Multisatellite Precipitation Analysis (TMPA) dataset (TRMM 2011) was used here due to the high spatial coverage (approximately 80%) of the tropical atmosphere and high temporal availability (Huffman et al. 2007). The TMPA dataset combines microwave-infrared measurements from various low earth orbit satellites into a global 3-hourly gridded analysis at 0.25° × 0.25° latitude–longitude resolution. Because of data availability,

precipitation rates from TMPA were obtained only for TCs between 1998 and 2014 located within 50° of the equator.

b. Methods

A database was created to combine information from the aforementioned datasets only at synoptic times (0000, 0600, 1200, and 1800 UTC). For consistency across basins, genesis was defined as the first instance of 17 m s^{-1} (i.e., tropical storm intensity). Data points corresponding to waves, disturbances, subtropical cyclones, extratropical cyclones, and TCs over land or within 24 h of landfall were not included in the database. These conditions result in 47 287 six-hourly data points (hereafter "events") associated with 2631 individual TCs. Events were considered separately because TCs can encounter different environments and experience different intensity changes over time. For each event, TC and environmental characteristics were obtained from IBTrACS, ERAI, CFSR, and the NOAA SST analyses. TC characteristics included variables derived or calculated from IBTrACS (e.g., intensity, latitude, translational speed) as well as the radius of outermost closed isobar (ROCI).[1] ROCI was calculated from the reanalysis by taking the average radius of the closed isobar (at 1-hPa intervals) farthest away from the TC center. In addition, various environmental characteristics that were investigated in previous studies (cf. section 1) were computed, including VWS, SST, precipitable water (PW), and lower- and middle-tropospheric relative humidity (RH).

Environmental characteristics were calculated from ERAI and CFSR using a similar approach as in statistical prediction models (e.g., DeMaria and Kaplan 1999). Given the large errors in TC location within both reanalysis datasets (Schenkel and Hart 2012), the TC center in ERAI and CFSR was identified via the absolute maximum[2] 850-hPa relative vorticity within a 500 km × 500 km box centered on the IBTrACS position. The vortex was removed from the wind field following the methods of Davis et al. (2008) and Galarneau and Davis (2013). In summary, the rotational and divergent wind components within a 500-km radius from the TC center were calculated with a Poisson equation and were subtracted from the total wind field. This method was used to ensure that VWS was representative of the environment rather than the TC itself. Figure 1 shows an example of the wind field before and after removing the vortex associated with Hurricane Earl at 0000 UTC 30 August 2010. After removing the kinematic component of the vortex, area-averaged quantities were calculated within a 500-km radius from the TC center. The only exception was the SST, which was obtained from the closest grid point of each TC location in the NOAA OI SST analysis. The SST value was retrieved from the analysis 3 days prior to TC passage in order to remove the effect of TC-induced ocean surface cooling. Maximum potential intensity (MPI) was calculated from the retrieved SST and thermodynamic profiles at the TC center using the algorithm of Bister and Emanuel (2002).

1) Intensity change time scale and classification

Once all variables were combined into one database, the lagged correlation between VWS magnitude and intensity was evaluated to pick a time period to identify and compare intensifying and nonintensifying events. This calculation was based on all events over water for at least 120 h to use a uniform sample size (14 778) at all lead times. Moreover, three different VWS definitions were used to account for the potential sensitivity of the lagged correlation to the VWS definition (Velden and Sears 2014). All definitions used the same vortex removal approach summarized in the previous subsection, but the difference was either the radii used for the area-averaged calculation (either 0–500 or 200–800 km) or the levels used to calculate VWS (either the winds at 200 and 850 hPa or the layer-averaged winds between 150–300 and 700–850 hPa). Regardless of the definition, the same relationship exists between VWS at 0 h and intensity up to 120 h later: a negative correlation exists at all lead times, with a peak correlation of −0.3 around 36–42 h (Fig. 2a). Given the similarities between VWS definitions, the rest of the calculations considered only the 500-km area-averaged vector difference between 200 and 850 hPa.

The lagged correlation suggests that TC intensity is most negatively affected by VWS during the 36–42-h period after a TC moves into a sheared environment; however, that analysis does not account for temporal changes of VWS. Persistence of VWS was tested by comparing the standard deviation of VWS magnitude to the root-mean-square error (RMSE) associated with assuming a constant VWS magnitude over time. The RMSE was defined as follows:

$$\mathrm{RMSE}(t) = \sqrt{\frac{\sum_{i=1}^{N} (V_{t_0,i} - V_{t,i})^2}{N}},$$

where V_{t_0} is the VWS magnitude at the beginning of the 120-h period, V_t is the VWS magnitude at each lead

[1] This metric was used because it can be determined from reanalysis rather than subjectively estimated, such as the radius of 34-kt (1 kt = 0.51 m s^{-1}) winds.

[2] This method provided the most robust and consistent identification of the TC center. Other methods, such as vorticity centroid, were not consistent across cases and basins.

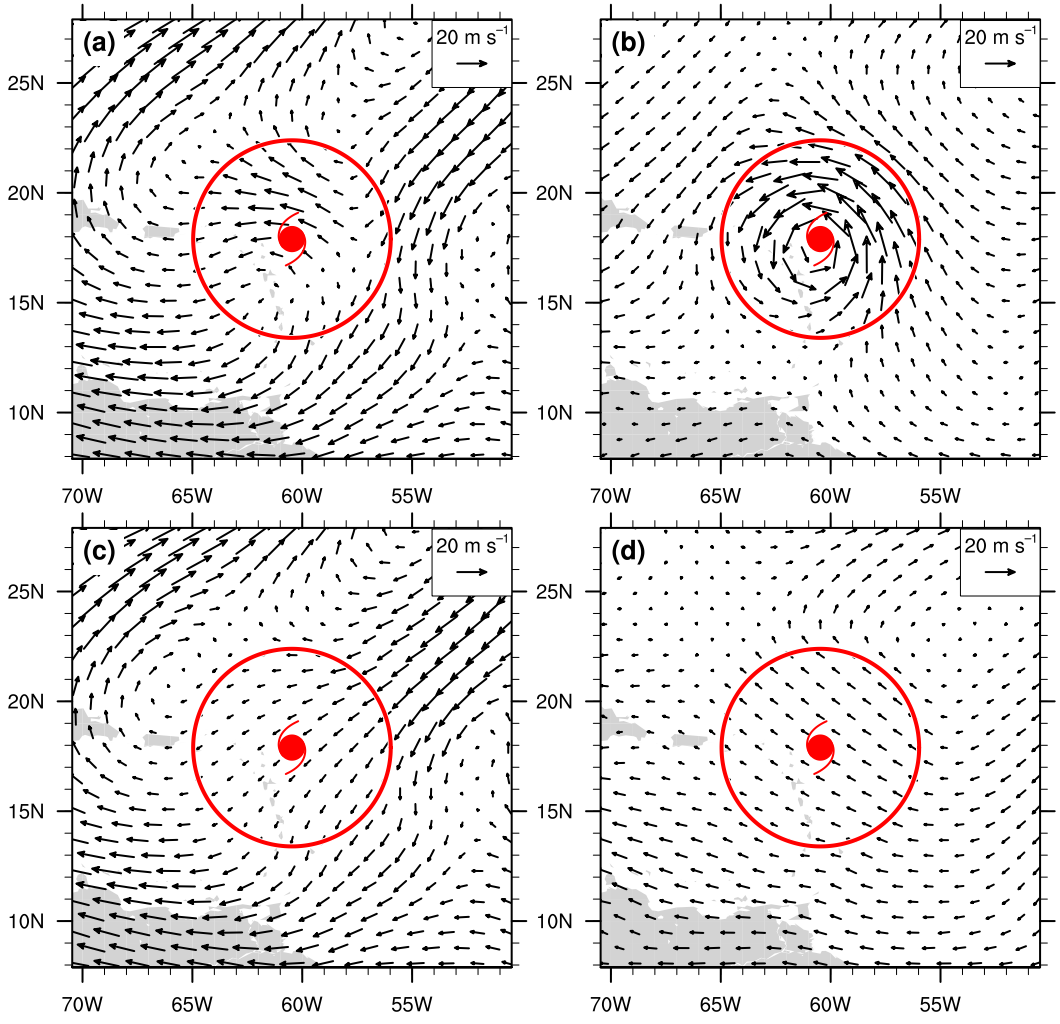

FIG. 1. Illustrative example of vortex removal methodology applied to Hurricane Earl (2010). (a),(c) 200- and (b),(d) 850-hPa winds at 0000 UTC 30 Aug 2010 (top) before and (bottom) after removing the vortex from the analysis. The red hurricane symbol and circle depict the center and the 500-km radius of Hurricane Earl.

time, and N is the sample size (14 778). Figure 2b shows that the standard deviation of VWS magnitude increases at a slower rate than the RMSE; while the standard deviation increases from 4.0 to 7.4 m s^{-1}, the RMSE increases from 0 to 9.0 m s^{-1} during the 120-h period. Consequently, the RMSE becomes larger than the standard deviation after 36 h, which indicates that a random drawing of VWS from climatology would be a better estimate than the initial VWS. Because this result indicates that VWS varies substantially over time, intensity changes were evaluated at different time periods no longer than 36 h. The focus here will be 24-h intensity changes, but other time periods were also considered to test the consistency and robustness of results.

Three groups of different intensity changes were identified for comparison: intensifying, steady-state, and weakening events. An event with an intensity change greater than 5 m s^{-1} was considered an intensifying event, whereas an event with an intensity change smaller than -5 m s^{-1} was considered a weakening event. Intensity changes between -5 and 5 m s^{-1} were classified steady-state events. A threshold of 5 m s^{-1} was used for each group because it represents the uncertainty of best-track intensity (Torn and Snyder 2012; Landsea and Franklin 2013), thus an absolute intensity change greater than 5 m s^{-1} should be detectable with current observational systems. All variables were evaluated at the beginning (t_0) of the intensity change period under the assumption that TC and environmental characteristics at t_0 influence the intensity at $t_0 + 24$ h. Time-averaged variables over the intensity change period were also considered to account for temporal evolutions;

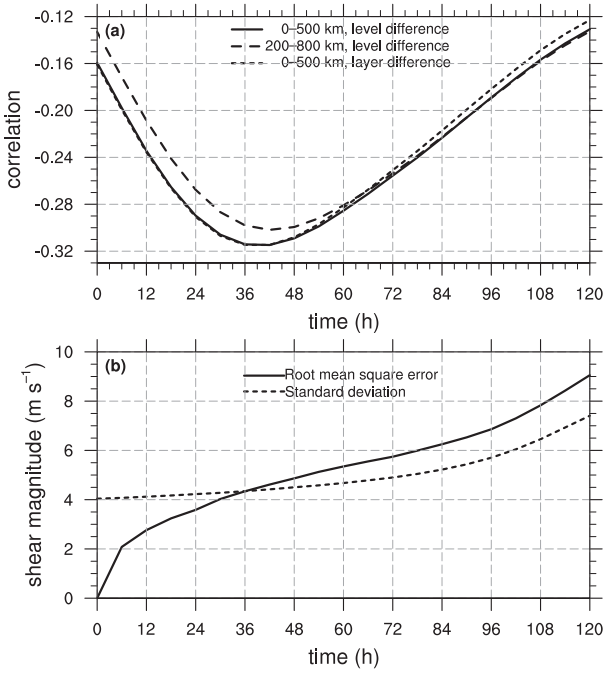

FIG. 2. (a) Time series of 6-hourly correlation between VWS at 0 h and intensity between 0 and 120 h. Lines represent different shear definitions: 0–500-km area-averaged differences between 200 and 850 hPa (solid), 200–800-km area-averaged difference between 200 and 850 hPa (long dashed), and 0–500-km area-averaged difference between 150–300- and 700–925-hPa layer-averaged winds (short dashed). (b) Time series of 6-hourly root-mean-square error (solid) and standard deviation (dashed) of 200–850-hPa VWS magnitude.

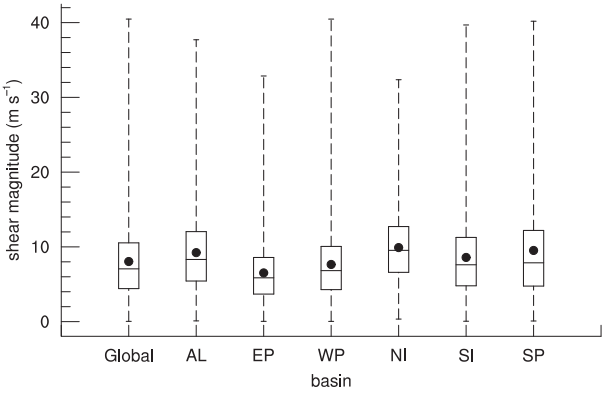

FIG. 3. Distributions of 200–850-hPa shear magnitude averaged between 0- and 500-km radius from each tropical cyclone center after vortex removal. Standard boxplots are used to summarize the distributions; whiskers extend from minimum to maximum, boxes extend from the 25th to the 75th percentile, horizontal lines within the boxes represent medians, and dots represent means of the distributions. The first boxplot from left to right represents the distribution of all events in the database, whereas the rest of the boxplots represent the North Atlantic (AL), eastern North Pacific (EP), western North Pacific (WP), northern Indian Ocean (NI), southern Indian Ocean (SI), and South Pacific (SP) basins.

however, those variables must be interpreted with caution because different intensity changes could alias onto time-averaged quantities.

2) MODERATE VWS DEFINITION

The database was further separated into three VWS categories: weak, moderate, and strong. Categories were defined based on percentiles of VWS experienced by all events in the database because no consistent definitions appeared in previous literature. Figure 3 shows the global and basin-based distributions of VWS magnitude constructed with all events over water for at least 24 h. All distributions are skewed toward small values, which are expected as weak VWS is a necessary condition for TC development (e.g., Gray 1968). The mean and median of the global distributions (7 and 8 m s^{-1}, respectively) fall within the range of VWS magnitudes associated with large uncertainty in TC intensity forecasts (Bhatia and Nolan 2013; Zhang and Tao 2013; Tao and Zhang 2015). To include those values into the moderate VWS category, the lower and upper bound of moderate VWS were defined as the 25th and 75th percentiles of the global distribution (approximately 4.5 and 11.0 m s^{-1}, respectively). Weak VWS was designated as the bottom 25th percentile (shear magnitudes smaller than 4.5 m s^{-1}), whereas strong VWS was defined as the top 25th percentile (shear magnitudes greater than 11.0 m s^{-1}). These definitions are representative for TCs in all basins because the medians and means of individual basins fall within 2.5 m s^{-1} from the global values despite the different ranges of VWS magnitudes across basins (Fig. 3).

The separation of VWS by percentiles provides a reasonable representation of moderate VWS—a range of VWS magnitudes that are neither too weak to have little influence on TC intensity nor too strong to halt intensification. Figure 4 shows normalized distributions of 24-h intensifying, steady-state, and weakening events for any VWS as well as separated by moderate, weak, and strong VWS. The distributions were normalized with respect to the number of events in each VWS category to facilitate comparison between categories. Such comparison reveals that the percentage of events that intensified under moderate VWS (27.4%) was nearly identical to the percentage of events that intensified under any VWS magnitude (25.1%; Fig. 4). By comparison, this percentage substantially increased (from 27.4% to 36.2%) or decreased (from 27.4% to 9.5%) when the VWS was weak or strong, respectively. Steady-state and weakening events also remained nearly the same under any or moderate VWS, but the percentages

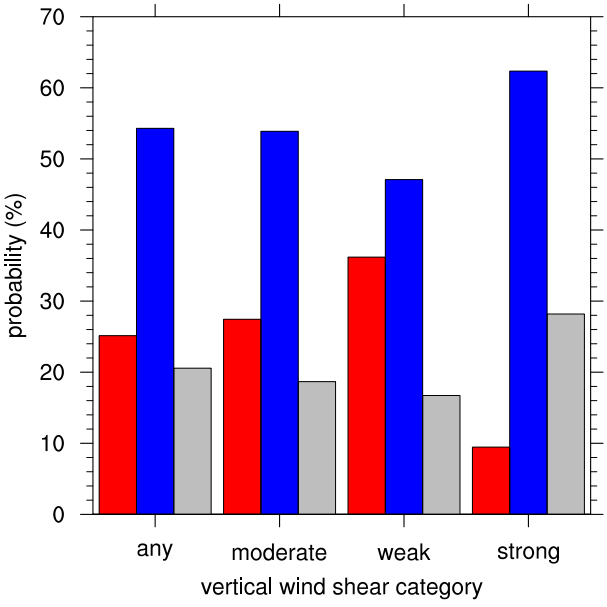

FIG. 4. Percentage of 24-h intensifying (red), steady-state (blue), and weakening (gray) events that encountered any, moderate, weak, or strong VWS. See text for a definition of each category.

of those events decreased or increased under weak or strong VWS, respectively. These differences in intensity rate distributions demonstrate that the 25th and 75th percentiles of the global VWS distribution are reasonable boundaries to distinguish between weak, moderate, and strong VWS. Only moderate VWS cases were considered in this study, reducing the sample size to 23 643 events.

3) ANALOGS SELECTION

To investigate which factors influence intensity changes under moderate VWS, a global statistical comparison of intensifying and steady-state events was performed.[3] An initial comparison of these groups revealed three characteristics of the dataset that could potentially bias the results. First, intensifying events had significantly weaker VWS than steady-state events (Fig. 5a). Given the large influence of VWS on intensity changes, this characteristic could mask the importance of other factors. Second, intensifying events were further from their MPI than steady-state events (Fig. 5b). This difference could alias onto both TC and environmental characteristics because intensification often follows genesis, when TCs are weak and over favorable environments. Third, intensifying events happened less often than steady-state events (Fig. 4b): intensifying events represent 27.4% (6489 events) of all cases that experienced moderate VWS, whereas steady-state events represent 53.9% (12 741 events) of those cases.

To address these issues, an analog approach was employed to compare two groups of equal size containing intensifying or steady-state events with comparable 200–850-hPa VWS magnitude and deviation from MPI. For each intensifying event, an analog steady-state event was randomly selected under the requirement that the VWS magnitude and deviation from MPI were within 1.25 and 5 m s^{-1}, respectively, from the corresponding values of the intensifying event. The thresholds for VWS magnitude and deviation from MPI were chosen after testing the algorithm for both speed and accuracy in selecting analog events. This process was repeated for each intensifying event that had an analog steady-state event, resulting in two groups of equal size (6420 events) with no significant differences in either VWS magnitude or deviation from MPI (Figs. 5c,d). The random drawing of analog groups was repeated 1000 times, such that each time two new groups of 6420 intensifying and 6420 steady-state events were randomly drawn from the database. This repetition was needed to consider all cases in the database, but the results were insensitive to the number of random drawings.

After the analog groups were selected, distributions and means of TC and environmental characteristics associated with intensifying and steady-state events were compared to identify factors conducive for intensification under moderate VWS. Statistical significance of the mean differences between the groups was evaluated with a bootstrap resampling approach similar to the algorithm of Rios-Berrios et al. (2016a). In short, a distribution of mean differences between two groups was created by randomly drawing two groups of equal size from the moderate VWS database. The distribution was used to test the null hypothesis that the mean difference between intensifying and steady-state events was the same as the difference between two randomly selected groups from the database. All statistical significance tests were evaluated at the 99.9% confidence level.

3. Statistical comparison of intensifying and steady-state events

a. *Tropical cyclone characteristics*

A comparison of TC characteristics reveals significant differences between intensifying and steady-state events at the beginning of the 24-h intensity change period. Intensifying events are slightly stronger than steady-state

[3] Weakening events were not considered because most of those events were high-latitude TCs close to extratropical transition or landfall.

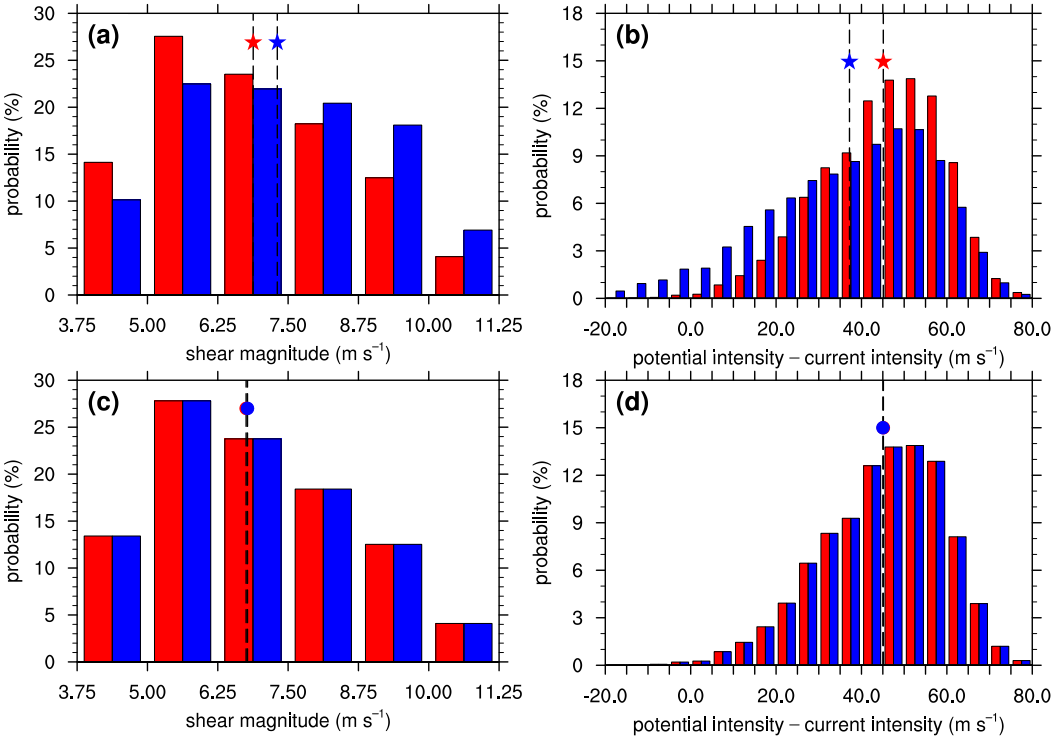

FIG. 5. Normalized distributions of (a),(c) 200–850-hPa shear magnitude and (b),(d) deviation from MPI of intensifying (red) and steady-state (blue) events. The top row shows the original distributions, whereas the bottom row shows the distributions of analogs with similar shear magnitude and deviation from MPI. The mean of each group is represented by a dashed line along with a star or circle, where a star indicates that the difference between the means is significant at the 99.9% confidence level.

events as shown by the distributions of maximum wind speed (Fig. 6a). The mean difference between the two subgroups is 4.02 m s^{-1} and is significant at the 99.9% confidence level. Intensifying events are also closer to the equator than steady-state events as shown by the comparison of absolute latitude (Fig. 6b). The mean difference between the groups is −1.36° and is statistically significant at the 99.9% confidence level. Intensifying events are also larger than steady-state events as revealed by the ROCI metric (Fig. 6c). Intensifying events have an average ROCI[4] that is 26.52 km significantly larger than the ROCI of steady-state events. However, this difference could result from the different latitudinal location of intensifying and steady-state events because ROCI is negatively correlated with latitude (not shown).

Another TC characteristic that should be evaluated is the translational speed because this variable could also influence intensity changes in sheared environments (Zeng et al. 2010; Rappin and Nolan 2012; Onderlinde and Nolan 2016). Comparing the translational speed between intensifying and steady-state events reveals that both groups move at nearly the same speed (Fig. 6d). Both groups have mean translational speeds of approximately 4.4 m s^{-1}, resulting in a small difference of 0.12 m s^{-1} between intensifying and steady-state events. Separating the translational speed into zonal and meridional components shows significant differences between the groups (Figs. 6e,f). On average, intensifying events have a more westward motion as revealed by the average zonal velocity difference of −0.54 m s^{-1}. Intensifying events also have a more northward motion, but the difference between the groups (0.24 m s^{-1}) is half the difference in the zonal component. These results suggest that the speed of motion is not a distinguishing factor between intensifying and steady-state events, though the zonal component of motion is more important.

These results are generally consistent when considering time-averaged TC characteristics, different intensity change periods, and different latitudinal regions

[4] Not all events had a closed isobar, which reduced the sample size for this variable.

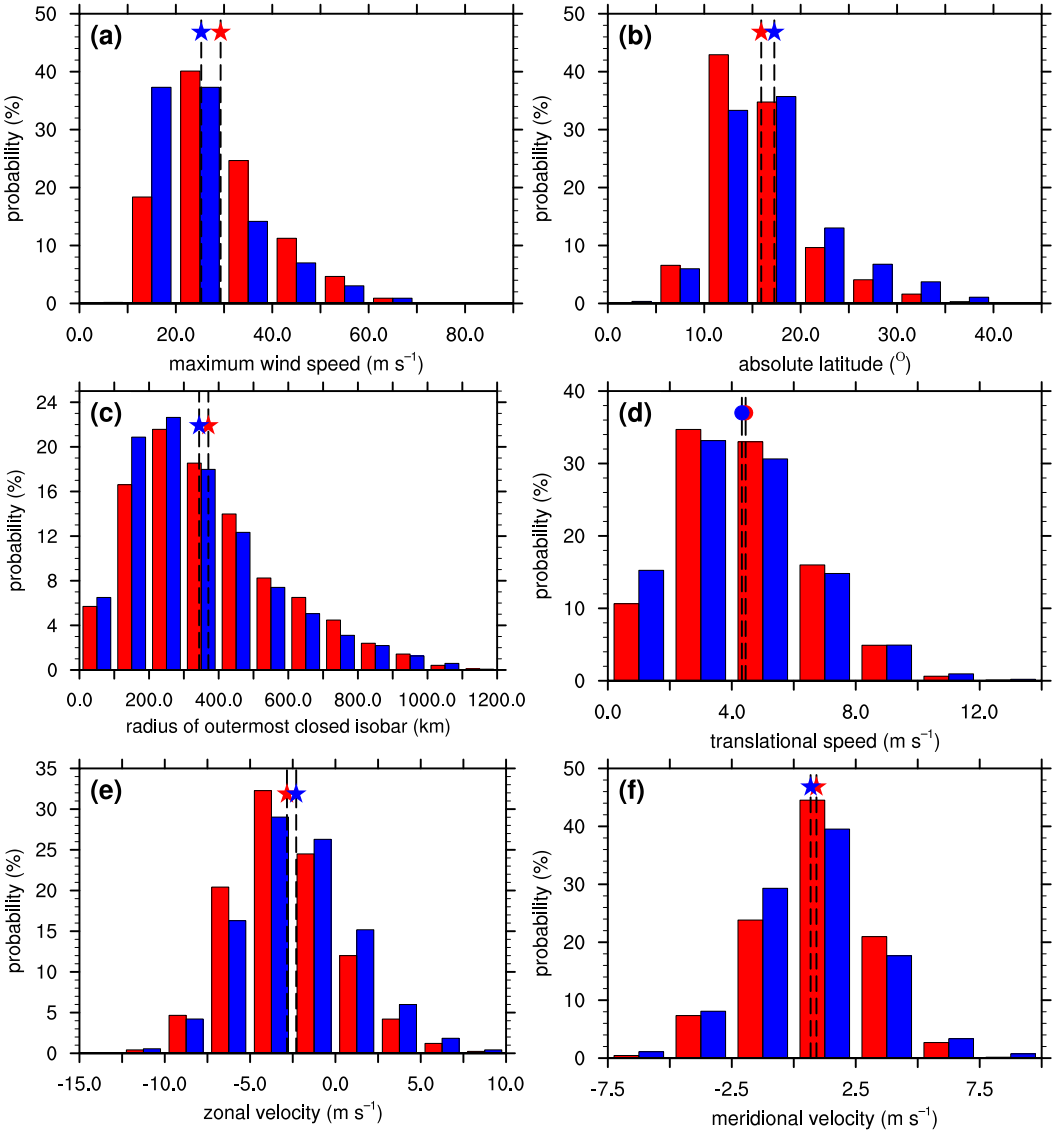

FIG. 6. Normalized histograms of (a) maximum wind speed, (b) absolute value of latitude, (c) ROCI, (d) tropical cyclone translational speed, and (e) zonal and (f) meridional components of tropical cyclone motion of intensifying (red) and steady-state (blue) events. The mean of each group is represented by a dashed line along with a star or circle, where a star indicates that the difference between the means is significant at the 99.9% confidence level.

(Fig. 7). Intensifying events are consistently stronger (Fig. 7a) and closer to the equator (Fig. 7b) than steady-state events. The relationship between TC size and intensity change is not consistent, but intensifying events are larger than steady-state events during 18-, 24-, and 30-h intensity changes (Fig. 7c). TC translational speed differences are generally insignificant at all periods considered (Fig. 7d), but the differences between the individual components consistently show more westward and northward motion (Figs. 7e,f). These results are most representative of TCs located equatorward of 20° latitude. Figure 8 shows the composite differences between the distributions of intensifying and steady-state events stratified by latitude. Intensifying events are initially stronger regardless of latitudinal location (Fig. 8a). Poleward of 20° latitude, the relationship between initial size and intensity change is unclear (Fig. 8b), but intensifying events are generally slower than steady-state events (Fig. 8c).

Overall, this comparison shows both consistent and inconsistent results with previous studies. On average, intensifying events are significantly stronger, closer to the equator, and larger than steady-state events. Theoretical and idealized modeling studies indicate that

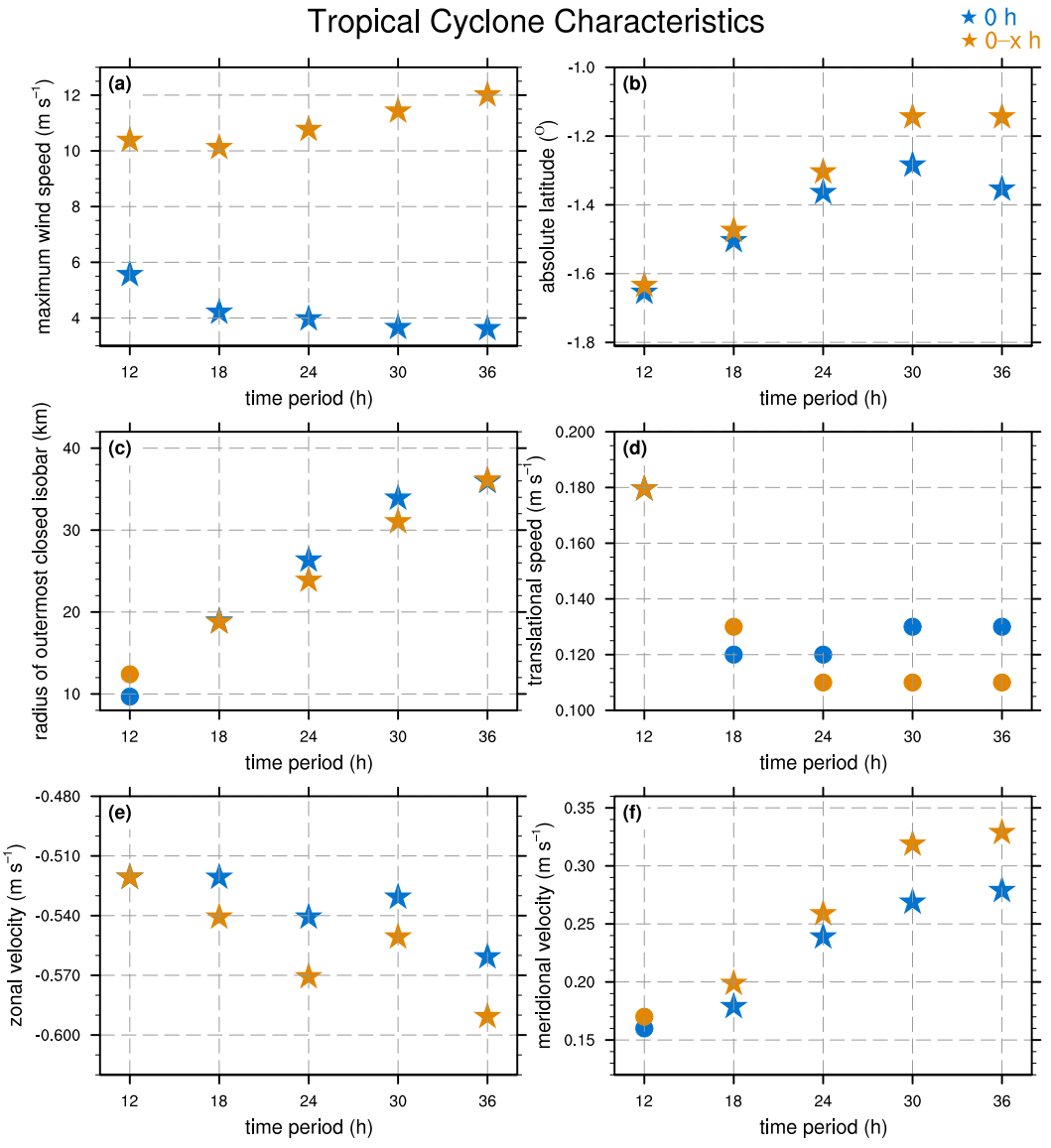

FIG. 7. Average differences between tropical cyclone characteristics of intensifying and steady-state events for various intensity change periods. Panels correspond to the panels in Fig. 6. Blue symbols depict differences at the beginning of each time period, whereas orange symbols depict time-averaged differences. Stars are shown when the average differences are statistically significant at the 99.9% confidence level and circles are shown otherwise.

strong and large TCs are more likely to withstand the effects of VWS than weak and small TCs (Jones 1995; DeMaria 1996; Reasor et al. 2004; Tang and Emanuel 2010; Riemer and Montgomery 2011; Tang and Emanuel 2012; Riemer et al. 2013; Reasor and Montgomery 2015). However, some of those studies also predict that TCs farther away from the equator have greater chances of overcoming the effects of VWS than TCs closer to the equator (Jones 1995; DeMaria 1996; Reasor et al. 2004; Reasor and Montgomery 2015). Figure 6a stands in contrast with those studies because intensifying events are closer to the equator than steady-state events. A possible explanation for this discrepancy is that other factors, such as thermodynamic conditions, can be more favorable for intensification closer to the equator. Recent modeling studies without VWS find that TCs at low latitudes intensify faster than TCs at high latitudes (Smith et al. 2015, and references therein); however, a recent study that included VWS found the opposite relationship regardless of thermodynamic environment (Zhou 2015). Thermodynamic environmental conditions will be compared in section 3b to clarify

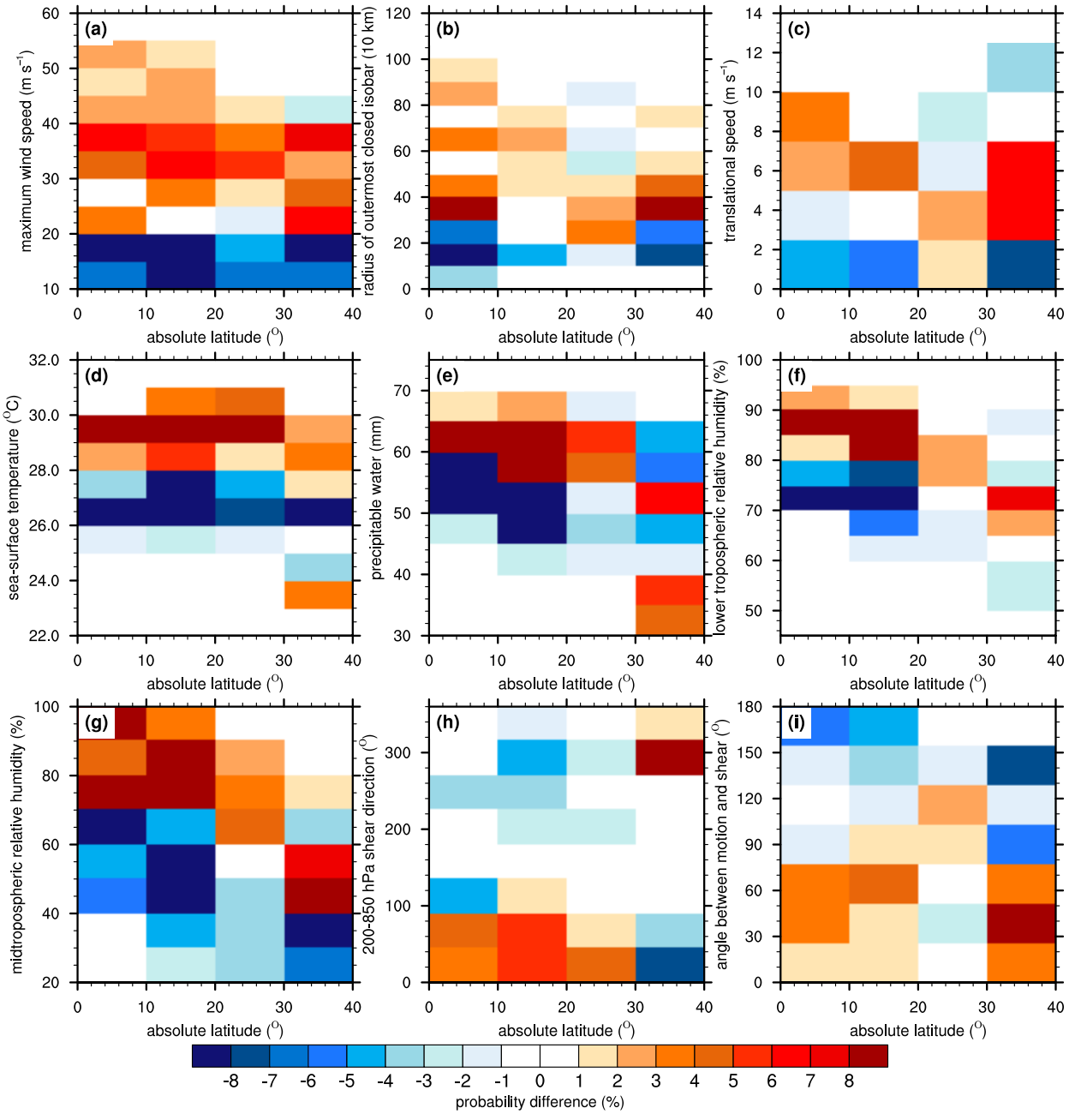

FIG. 8. Normalized distribution differences between intensifying and steady-state events stratified by latitude. Panels show the percentage difference at each bin (shading, %) for (a) maximum wind speed, (b) ROCI, (c) translational speed, (d) SST, (e) PW, (f) lower-tropospheric RH, (g) middle-tropospheric RH, (h) 200–850-hPa shear direction, and (i) angle between 200–850-hPa shear and tropical cyclone motion vectors.

the discrepancies among the current study and other studies.

b. Thermodynamic environmental characteristics

A comparison of thermodynamic environmental characteristics at the beginning of the 24-h intensity change period also shows statistically significant differences between intensifying and steady-state events (Fig. 9). Intensifying events move over significantly warmer SSTs than steady-state events as evidenced by the mean SST difference of 0.82°C (Fig. 9a). Environmental PW is also more favorable for intensifying events as the mean PW difference between the groups is 3.48 mm and is significant at the 99.9% confidence

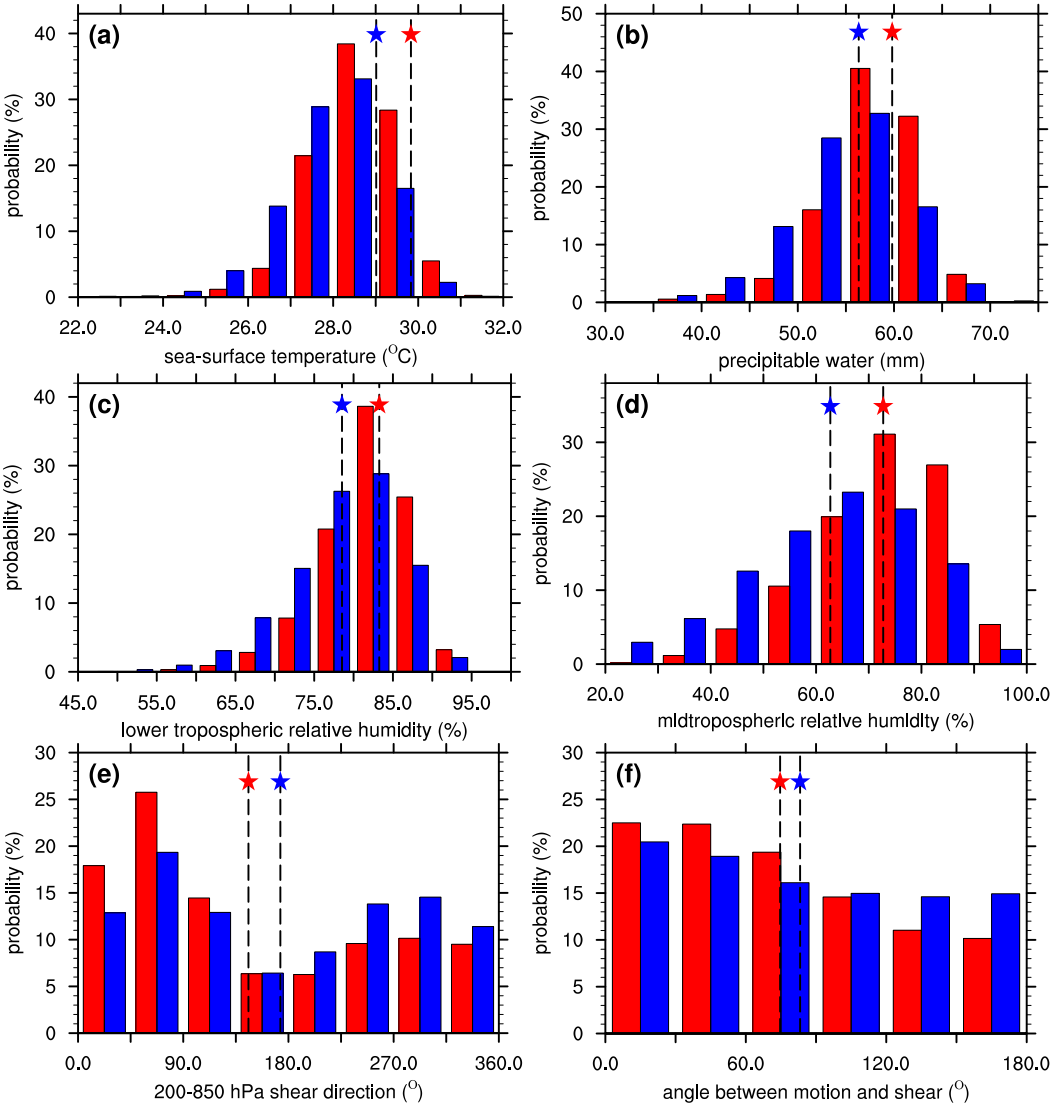

FIG. 9. Normalized distributions of (a) SST, (b) PW, (c) lower-tropospheric RH, (d) middle-tropospheric RH, (e) 200–850-hPa shear direction, and (f) angle between 200–850-hPa shear and tropical cyclone motion vectors of intensifying (red) and steady-state (blue) events. The mean of each group is represented by a dashed line along with a star or circle, where a star indicates that the difference between the means is significant at the 99.9% confidence level.

level (Fig. 9b). Given that PW is a vertically integrated quantity, RH must be evaluated at different vertical levels to determine the layer with greatest contribution to the PW discrepancies. Lower- and middle-tropospheric RH were evaluated as the 900–600- and 400–600-hPa layer averages, respectively (Figs. 9c,d). In the lower troposphere, the mean RH of intensifying events is 4.73% significantly larger than the mean RH of steady-state events (Fig. 9c). The mean difference between the middle-tropospheric RH of both groups is twice as large; intensifying events have 10.04% significantly larger RH than steady-state events (Fig. 9d).

These results are consistent at different intensity change periods, but some important variations appear for different latitudinal locations. At all time periods considered, intensifying events have more favorable thermodynamic conditions characterized by warmer SSTs (Fig. 10a), greater PW (Fig. 10b), and greater RH both in the lower and middle troposphere (Figs. 10c,d). The larger differences between time-averaged and 0-h PW and RH could result from the fact that intensifying events are becoming stronger and potentially moistening more their environments. SST and midtropospheric RH are consistent distinguishing factors of

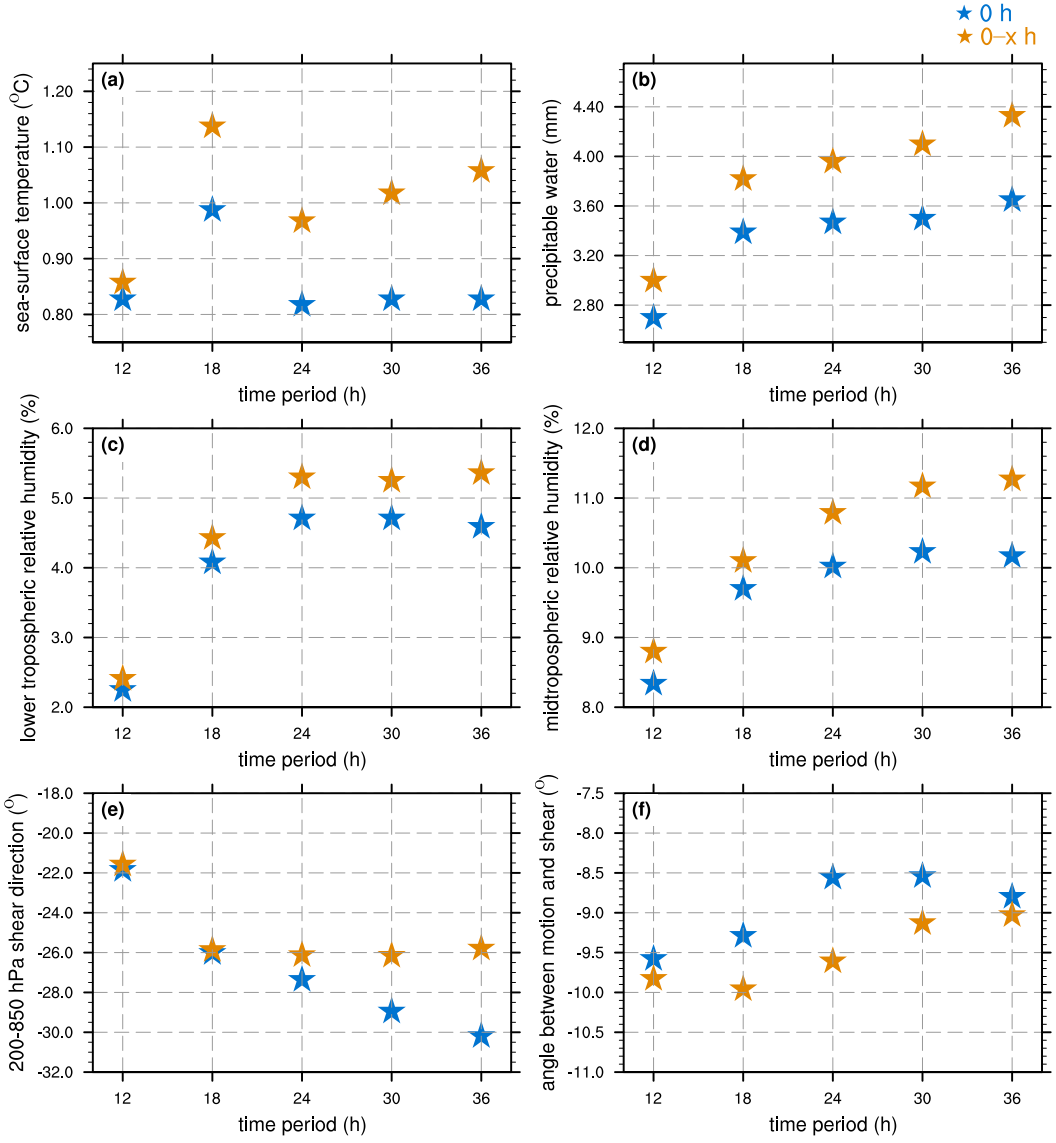

FIG. 10. Average differences between environmental characteristics of intensifying and steady-state events for various intensity change periods. Colors and symbols are as in Fig. 7, and panels correspond to the panels in Fig. 9.

intensifying and steady-state events regardless of latitudinal locations (Figs. 8d,g); however, PW and lower-tropospheric RH appear to favor intensification primarily equatorward of 30°. Intensifying events poleward of 30° have less PW and smaller lower RH than steady-state events (Figs. 8e,f), suggesting that different processes modulate the chances of intensification at high latitudes.

These results indicate that thermodynamic aspects of the environment largely influence TC intensity changes under moderate VWS. Overall, these results are consistent with previous observational (Molinari et al. 2004, 2006; Shelton and Molinari 2009; Nguyen and Molinari 2012) and modeling studies (Rios-Berrios et al. 2016a,b) that investigated the intensification of individual TCs. These results are also consistent with previous theoretical and idealized modeling studies that demonstrated the crucial role of near-TC moisture on intensity changes in sheared environments (Tang and Emanuel 2010; Riemer et al. 2010; Tang and Emanuel 2012; Tao and Zhang 2014). Nevertheless, Rios-Berrios et al. (2016a,b) emphasized the importance of the three-dimensional moisture distribution during intensity changes of sheared TCs. Environmental RH differences between intensifying and steady-state events must be further evaluated to determine if there is a preferred

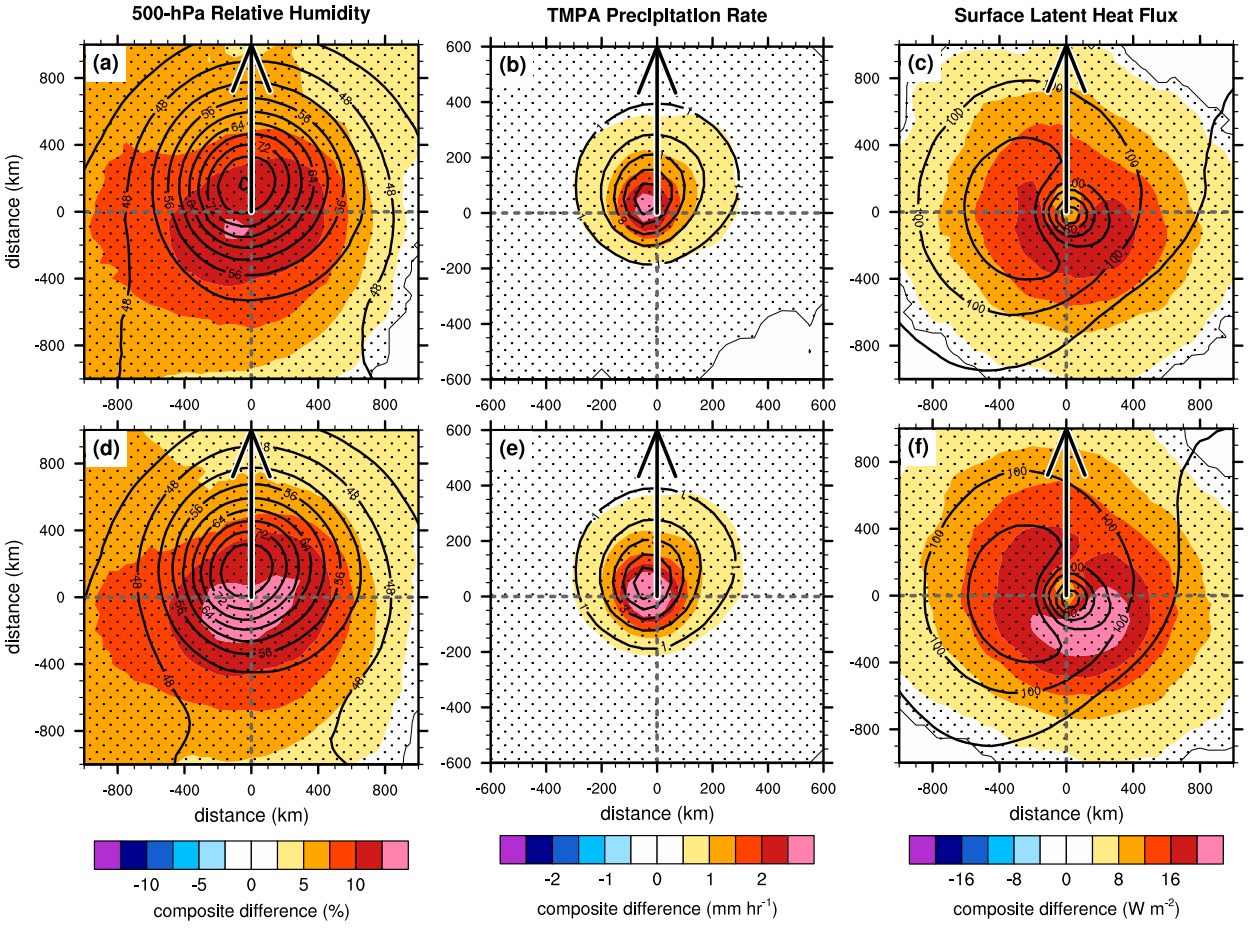

FIG. 11. Storm-centered, shear-relative analyses of (a),(d) 500-hPa RH (%); (b),(e) precipitation rate (mm h^{-1}); and (c),(f) surface LHF (W m^{-2}) at (top) 0 h and (bottom) averaged between 0 and 24 h. Black contours represent the mean of all intensifying and steady-state events, shading represents the composite difference between intensifying and steady-state events, and the stippling pattern represents statistically significant differences at the 99.9% confidence level. All fields were rotated with respect to the 200–850-hPa shear vector such that the shear vector (black and white arrow) points along the positive ordinate.

radius and azimuth of enhanced RH that favors intensification.

A storm-centered, shear-relative framework was employed to assess the spatial distribution of RH differences between intensifying and steady-state events. In this framework, fields are centered on the 850-hPa TC center in the reanalysis and rotated into a natural coordinate framework based on the 200–850-hPa VWS direction. Global composites were created by flipping the latitude of Southern Hemisphere fields to account for shear-relative asymmetries (Chen et al. 2006). Figure 11 shows fields in this storm-centered, shear-relative framework, where the ordinate represents downshear (positive values) or upshear (negative values) distance and the abscissa represents upwind (positive values) or downwind (negative values) distance with respect to the VWS vector. By combining both hemispheres into one global framework, shear-relative quadrants are defined as follows (counterclockwise from top right quadrant): downshear upwind, downshear downwind, upshear downwind, and upshear upwind.

An evaluation of storm-centered, shear-relative RH revealed the largest differences on the 500-hPa level; therefore, the following discussion focuses on that level (Figs. 11a,d). The mean ERAI fields (black contours) contain the well-documented wavenumber-1 asymmetry of sheared TCs (Corbosiero and Molinari 2002; Chen et al. 2006; Hence and Houze 2011; DeHart et al. 2014). Large RH values (up to 80%) are evident in the downshear half, with smaller values (up to 72%) in the upshear half. Composite differences between the groups (shading) reveal that intensifying events have significantly greater RH for all azimuths both at the beginning

(Fig. 11a) and during the intensification period (Fig. 11d). These differences suggest that intensifying events are less prone to dry air intrusions, which agrees with previous literature (Riemer and Montgomery 2011; Riemer et al. 2013; Tang and Emanuel 2012) because intensifying events are also stronger and larger than steady-state events. Furthermore, the largest differences between the groups appear within the inner 200 km of the upshear half, where intensifying events have up to 12.5% greater RH than steady-state events (Fig. 11a). These differences amplify in both magnitude and spatial coverage during the intensification period (Fig. 11d). As the upshear half is typically characterized by dry air and subsidence, this result suggests that intensifying events have a more symmetric RH field than steady-state events. A comparison of the wavenumber-1 structure confirms that intensifying events have a more symmetric midtropospheric RH (not shown); however, symmetry differences could result from different TC structure, different distribution of environmental moisture, or a combination of both TC and environmental factors.

A more symmetric midtropospheric RH distribution likely favors more symmetric convection; however, this hypothesis cannot be assessed with reanalysis datasets because of the coarse resolution and the use of a cumulus parameterization scheme in the underlying model. Instead, precipitation rate estimates were obtained from the TMPA dataset to diagnose rainfall differences between intensifying and steady-state events. Figures 11b,e show a comparison of precipitation rates for intensifying and steady-state events with available data (1998–2014). As in the composite analysis of RH, the mean TMPA fields depict a wavenumber-1 asymmetry with larger precipitation rates in the downshear half than in the upshear half. Composite differences between intensifying and steady-state events confirm that intensifying events have higher precipitation rates than steady-state events. Significant differences are evident at all azimuths, but especially within a 200-km radius, where intensifying events have up to 3 mm h^{-1} greater precipitation rates than steady-state events (Fig. 11b). Consistent with the RH differences, composite precipitation rate differences amplify during the intensification period (Fig. 11e). There is a slight preference for greater differences in the downwind quadrants. That region is characterized by the largest amplitude of wavenumber-1 rainfall asymmetry (Chen et al. 2006), suggesting that intensifying events have stronger and more symmetric convection.

Even though both the RH and precipitation rate comparison suggest more symmetric convective activity in intensifying events, the azimuthal distribution of surface latent heat fluxes (LHF) could also influence the symmetry of convection (Rappin and Nolan 2012; Onderlinde and Nolan 2016). Surface LHF were computed from the reanalysis via the bulk aerodynamic formula:

$$\mathrm{LHF} = L_v c_k \rho_d U_{10} (q^*_{\mathrm{SST}} - q),$$

where L_v is the latent heat of vaporization, c_k is the enthalpy exchange coefficient, ρ_d is the dry air density, U_{10} is the 10-m wind speed, q^*_{SST} is the saturated specific humidity at SST, and q is the 2-m specific humidity. An evaluation of the fluxes shows that intensifying events have significantly greater surface LHF than steady-state events at all azimuths both at the beginning and during the intensity change period (Figs. 11c,f). The largest differences appear in the upshear upwind quadrant, where intensifying events initially have up to 20 W m^{-2} significantly stronger surface LHF than steady-state events (Fig. 11c). Composite differences also amplify during the intensification period (Fig. 11f), indicating that surface LHF are consistently providing conducive conditions for the azimuthal propagation of convection around intensifying events. These results are consistent with previous modeling studies (Rappin and Nolan 2012; Onderlinde and Nolan 2016), which showed that enhanced surface LHF in the upshear semicircle promote the axisymmetrization of convection during intensification in sheared environments.

Notwithstanding the significant RH, precipitation rate, and surface LHF differences between intensifying and steady-state events, the presence of air masses with different RH does not solely explain intensity changes. As previous studies have indicated, a mixing mechanism is necessary for dry air to dilute convection and, hence, influence intensity changes (Riemer and Montgomery 2011; Tang and Emanuel 2012; Ge et al. 2013). Two potential hypotheses can be motivated by the RH differences shown in Fig. 11: 1) storm-relative flow differences between the groups can modulate the import of dry air or export of moist air, and 2) a stronger primary circulation in intensifying events can favor the recirculation of moist air around the TCs.

c. *Kinematic environmental characteristics*

Storm-centered, shear-relative composites of storm-relative radial and tangential winds were considered to assess asymmetries in the kinematic field and to relate those asymmetries to the RH differences (Fig. 12). The composite 500-hPa storm-relative radial wind depicts inflow downwind of the shear vector and outflow upwind of the shear vector (black contours in Figs. 12a,c). This inflow–outflow setup rotates with height such that at 850 hPa the inflow appears in the downshear half and

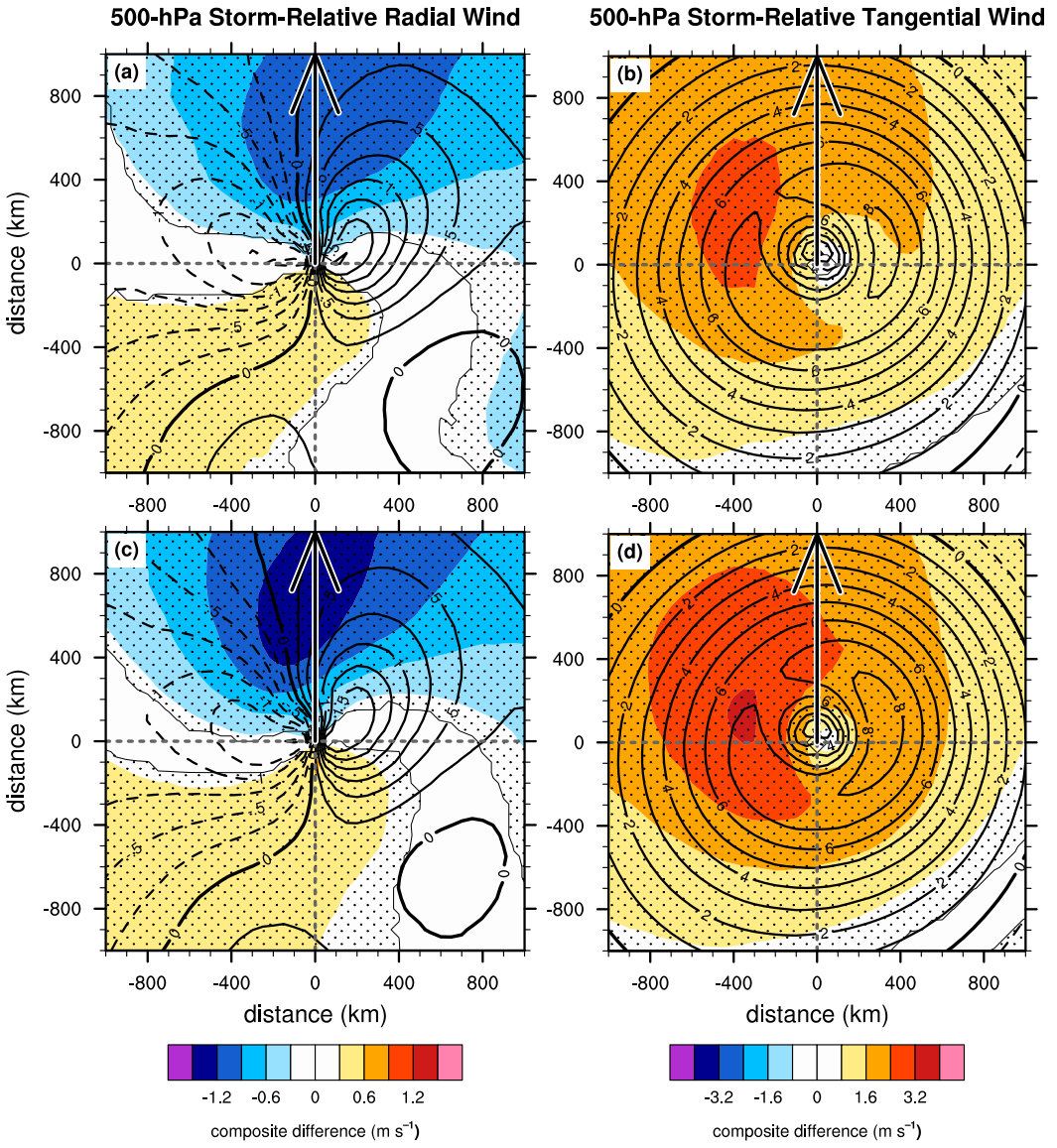

FIG. 12. As in Fig. 11, but for (a),(c) 500-hPa storm-relative radial wind ($m\,s^{-1}$) and (b),(d) 500-hPa storm-relative tangential wind ($m\,s^{-1}$).

outflow appears in the upshear half (not shown). This pattern is consistent with airborne Doppler radar composites of the kinematic field of sheared TCs shown by Reasor et al. (2013) even though that study only considered the inner-core region. The storm-relative tangential wind at 500 hPa also shows asymmetries, with the strongest tangential wind located upwind of the shear vector (black contours in Figs. 12b,d). This pattern also rotates with height, such that at 850 hPa the maximum tangential wind is upwind of the shear vector (not shown).

Comparing intensifying and steady-state events shows statistically significant differences between the storm-relative flow of the two groups. The storm-relative radial wind exhibits a storm-centered dipole with negative differences in the downshear half and positive differences in the upshear half (shading in Figs. 12a,c). This pattern, which also appears in the lower troposphere (not shown), indicates that intensifying events have stronger inflow in the downshear half and stronger outflow in the upshear half. A wavenumber-1 asymmetry was evident in the RH composite field (Figs. 11a,d), thus the stronger inflow is located in a region of higher RH than the region of stronger outflow. Intensifying events also have stronger storm-relative tangential winds at all azimuths, but the largest differences ($3.2\,m\,s^{-1}$) appear downwind of the shear vector (shading in Figs. 12b,d). Given that the composite mean shows

maximum tangential wind upwind of the shear vector, the location of largest differences suggests that intensifying events have a stronger, broader, and more symmetric midlevel circulation than steady-state events. These different storm-relative flow configurations, together with the RH composites, suggest that intensifying events are importing more moist air toward the TC, exporting more dry air away from the TC, and recirculating air with higher RH around the TC.

The existence of significant differences in storm-relative winds hints at differences between the wind profiles and/or the large-scale structure of the TC vortex. Intensifying and steady-state events considered here have the same 200–850-hPa VWS magnitude (cf. Fig. 5c), but not necessarily the same VWS direction. Previous studies suggest that easterly VWS can be more favorable to intensification than westerly VWS (Black et al. 2002; Ritchie and Frank 2007; Zeng et al. 2010). However, subsequent studies suggest that the angle between VWS and TC motion is more important, such that a TC moving in opposite direction to the VWS vector is more likely to intensify than a TC moving in the same direction as the VWS (Rappin and Nolan 2012; Onderlinde and Nolan 2016). Furthermore, the profile of environmental winds between 200 and 850 hPa could also cause different vortex-scale kinematic asymmetries (Finocchio et al. 2016). Another possibility is that the differences in storm-relative flow result from the response of the TC vortex (e.g., tilt) to the VWS (Jones 2000). While the datasets employed in this study may be sufficient to test the hypothesis related to the wind profile, a higher-resolution dataset is needed to evaluate differences related to vortex structure.

Two basic metrics can be used to assess variability in the wind profile: the 200–850-hPa VWS direction and the angle between the 200–850-hPa VWS and TC motion. The distribution of 200–850-hPa VWS direction shows two relative maxima: one corresponding to easterly VWS and another for westerly VWS (Fig. 9e). On average, intensifying events have more easterly VWS and less westerly than steady-state events as indicated by the mean, significant difference of −27.29° between the groups. This result is consistent for all basins even though the mean VWS direction varies per basin (not shown) and is also consistent over different time periods (Fig. 10e). A latitudinal dependency appears for this result as westerly VWS is more favorable for intensification poleward of 30° latitude (Fig. 8g). The distribution of the angle between VWS and TC motion also shows significant differences between the subgroups, albeit contrary to the result from previous studies (Fig. 9f). On average, intensifying events have a significantly smaller angle between VWS and TC motion than steady-state events, which indicates that intensifying events are more likely to experience VWS in the same direction as motion. This relationship is consistent for other intensity change periods (Fig. 10f) as well as for all latitudinal locations (Fig. 8i).

These results suggest that easterly VWS and westward TC motion are more favorable for intensification. The result about VWS direction is consistent with previous studies, but VWS direction is negatively correlated with environmental thermodynamics (not shown). Such correlation indicates that environments with easterly VWS are also characterized by warm SSTs and high PW. The TC motion–VWS result contradicts idealized modeling studies that suggest TC motion opposite to the VWS direction is more favorable for development and intensification. A challenging aspect of comparing results is that intensifying and steady-state events have nearly similar translational speed (cf. Figs. 6d–f), whereas modeling studies prescribed two or more different TC motion scenarios in their simulations (e.g., easterly vs westerly mean flow). Details of the wind profiles between 200 and 850 hPa must be further evaluated to determine if other factors associated with the environmental winds, such as shape or VWS layer, distinguish intensifying and steady-state events.

A *K*-means clustering analysis (MacQueen 1967) was employed to investigate variability among environmental zonal and meridional wind profiles. This analysis was necessary because this study focuses on global data; therefore, it is possible that variability among the background wind profiles between basins could mask out differences between intensifying and steady-state events. The 200–850-hPa VWS direction was used as the metric to cluster wind profiles after several tests with different variables, including the magnitude of storm-relative flow at different levels and the variance of zonal and meridional environmental winds. One of the caveats of the *K*-means algorithm is that the number of clusters should be specified a priori. To determine the optimal number of clusters, the cohesiveness of the clusters was measured via the ''silhouette'' metric (Rousseeuw 1987):

$$S = \frac{\min(b) - a}{\max[a, \min(b)]},$$

where a is the average distance between a point and all other points in the same cluster, and b is the average of the average distance between a point and all other points in other clusters. Positive silhouette values close to 1 represent cohesive clusters. The *K*-means algorithm was applied using different number of clusters, resulting in mean silhouette values between 0.55 for six clusters

TABLE 1. Summary of each cluster of environmental wind profiles. (from left to right) The first column indicates the cluster number, the second column indicates the mean 200–850 hPa VWS direction, the third column provides the number of events (N) in each cluster, and the fourth and fifth columns provide the number of intensifying (N_1) and steady-state (N_2) events, respectively, in each cluster.

Cluster	Centroid VWS direction (°)	N	N_1	N_2
1	127.7	1812	942	870
2	329.7	1781	803	978
3	74.5	3147	1744	1403
4	28.5	2338	1369	969
5	209.0	1626	678	948
6	270.5	2136	884	1252

and 0.72 for two clusters. Six clusters were specified because the mean silhouette was relatively high and the clusters contained comparable number of events (Table 1).

Clusters identified with the K-means algorithm were used to compare the environmental storm-relative winds of intensifying and steady-state events. Six distinctive VWS directions were identified: 1) southeasterly (Fig. 13a), 2) northwesterly (Fig. 13b), 3) easterly (Fig. 13c), 4) northeasterly (Fig. 13d), 5) southwesterly (Fig. 13e), and 6) westerly (Fig. 13f). Composite hodographs of storm-relative environmental winds show no appreciable differences between intensifying and steady-state events in each cluster; the composite hodograph of intensifying events roughly matches the composite hodograph of steady-state events (Fig. 13). Furthermore, the mean TCREH from the environmental wind profiles is close to zero, which results in a small difference between the groups ($0.5\,m^2\,s^{-2}$, not shown). Wind variations with height are also remarkably similar between the groups, with no clear indication of distinct layers of VWS in intensifying versus steady-state events. Additional analyses with different methodologies (e.g., principal component analysis), with smaller datasets (e.g., only one basin), and with time-averaged wind profiles yielded similar conclusions (not shown).

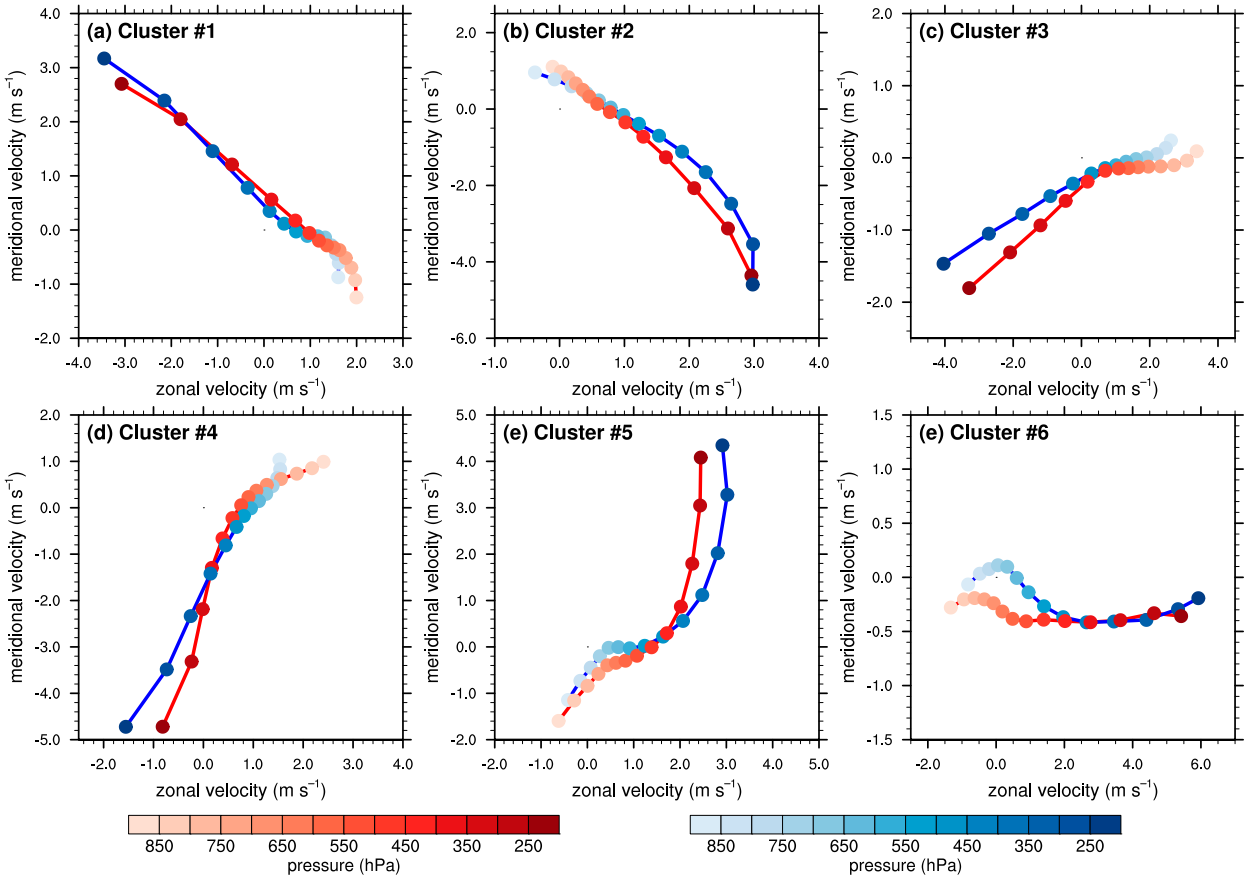

FIG. 13. Composite hodographs of environmental storm-relative winds for two sets of analog intensifying (red) and steady-state (blue) events. Filled circles depict composite winds every 50 hPa from 850 to 200 hPa. Clusters are shown by 200–850-hPa shear direction: (a) southeasterly, (b) northwesterly, (c) easterly, (d) northeasterly, (e) southwesterly, and (f) westerly.

These results indicate that the shape of the environmental wind profile has little ability to distinguish intensifying and steady-state events under moderate VWS. A potential implication of this result is that the time scale needed for the environmental winds to have an effect of intensity change is longer than the time scale of VWS itself. Onderlinde and Nolan (2014) found the largest impact of TCREH on intensity change for time periods between 96 and 168 h, whereas Finocchio et al. (2016) found the largest intensity variance due to VWS height between 36 and 72 h. Those studies also considered TC intensity changes with constant VWS during 120 h, which might not be reasonable for real-world TCs. As was shown in Fig. 2b, the RMSE associated with the assumption of constant VWS becomes larger than the standard deviation of VWS after 36 h, thus indicating that environmental winds in the real atmosphere evolve at a faster rate than the time scales employed by idealized modeling studies. Zeng et al. (2010) and Wang et al. (2015) considered similar time scales as in this study; however, those studies only considered correlation analyses for individual basins and for all VWS magnitudes. Future studies may want to consider idealized simulations that allow temporal VWS variations to elucidate these discrepancies regarding the sensitivity of TC intensity to the shape of the wind profile.

4. Summary and conclusions

The goal of this study was to identify TC and environmental characteristics that aid intensification under moderate VWS. A database was created to combine best tracks and environmental diagnostics for all TCs that reached at least tropical storm intensity and remained tropical and over water during a 24-h period between 1982 and 2014. Using this comprehensive database, moderate VWS was defined as 4.5–11.0 $m\,s^{-1}$, which represents the 25th–75th percentiles of the global distribution of 200–850-hPa VWS magnitude. This definition captured the essence of moderate VWS—a range of VWS magnitudes that are neither too weak to have little impact on intensity changes nor too strong to halt intensification. Two groups with different intensity changes under moderate VWS were compared: events with intensity changes greater than 5 $m\,s^{-1}$ (named intensifying events) and events with intensity changes between −5 and 5 $m\,s^{-1}$ (named steady-state events). The comparison focused on short-term (e.g., 24 h) intensity changes because an analysis of VWS persistence showed that VWS varies substantially over time. A unique analog approach was employed to statistically compare intensifying and steady-state events with nearly identical VWS magnitude and deviation from MPI. This approach was necessary to identify factors—other than VWS and deviation from MPI—that favored intensification under moderate VWS.

The global statistical comparison of TC and environmental characteristics showed significant differences between intensifying and steady-state events. Intensifying events were significantly stronger, closer to the equator, larger, and moving with a more westward motion than steady-state events. Furthermore, intensifying events moved within environments with warmer SSTs, greater PW, and more easterly VWS than steady-state events. These variables are correlated with each other, such that both thermodynamic and kinematic aspects of the environment work together to provide more favorable conditions for intensification under moderate VWS. Environmental characteristics were further examined to find the preferred horizontal and vertical location of thermodynamic differences between the groups. Storm-centered, shear-relative fields revealed that intensifying events had greater midtropospheric RH and surface LHF at all azimuths, but especially in the upshear half. These results hinted at more favorable environments for heavy and symmetric precipitation in intensifying events, which was confirmed with composite differences of satellite-estimated rainfall rates.

Additional analysis revealed that intensifying and steady-state events also had different kinematic structures. Intensifying events had stronger midlevel storm-relative inflow within the downshear half and stronger midlevel storm-relative outflow within the upshear half. This pattern was superposed with a wavenumber-1 asymmetry of RH, thus indicating that intensifying events were importing more moist air toward the TCs and exporting more dry air away from the TCs. Intensifying events also had stronger midlevel storm-relative tangential winds, which could also contribute to recirculating moist air around the TC. Altogether, these findings agree with previous modeling work that showed that strong and large TCs could be less prone to dry air intrusions than weak and small TCs (Riemer and Montgomery 2011; Tang and Emanuel 2012; Riemer et al. 2013).

Kinematic differences between the groups were hypothesized to be related to the vertical profile of environmental winds, the structure of the TC vortex, or a combination of both the environmental winds and the vortex structure. Results indicate that the latter is the most likely reason because the analysis did not show clear systematic differences between the wind profiles of

intensifying and steady-state events. Vortex structure differences could not be evaluated due to the coarse resolution of the dataset. Based on the composite differences of storm-relative flow, a plausible hypothesis is that intensifying events are both stronger and less tilted than steady-state events. Intensifying events had stronger tangential winds and associated stronger circulation at all vertical levels (not shown). Moreover, intensifying events had a stronger inflow in the downshear half, which would result in flow opposite to the VWS vector and potentially opposite to the vortex tilt. This hypothesis should be tested in the future with high-resolution composites of vortex tilt. Regardless of the reasoning for the different storm-relative winds, results show that the combined effects of RH asymmetries and storm-relative winds can modulate intensity changes under moderate VWS.

The lack of systematic differences between the environmental wind profiles contradicts previous modeling studies that considered the sensitivity of intensity changes to properties of the environmental wind profiles (Onderlinde and Nolan 2014; Finocchio et al. 2016). The underlying conclusions of those studies were similar; different environmental winds led to different tilt configurations, which led to different convective distributions and different timings of vortex realignment. Other studies reached similar conclusions by changing other properties of the environment such as the location of dry air (Ge et al. 2013) or the boundary layer moisture (Tao and Zhang 2014). The similarity between conclusions in spite of the different methods suggests that the underlying key to intensification is the axisymmetrization of convection and vortex realignment. However, all the aforementioned studies employed constant VWS through the entire simulation period. Additional work, preferably within a modeling framework that allows temporal variations of VWS, is needed to elucidate the mechanisms driving intensification under moderate VWS.

Several caveats may limit the results presented in this study. First, the results presented here relied on reanalysis datasets, which are not true representations of the atmosphere and only capture the large-scale aspects of TCs. The consistency between two reanalysis datasets (i.e., ERAI and CFSR) lends confidence on the results, but additional efforts are needed to link the large-scale results to vortex-scale and convective-scale processes. Second, some of the differences found here were small and probably difficult to measure with current observational systems. Third and last, all basins were considered together even though TC and environmental characteristics may vary from basin to basin. Ongoing work is repeating the analysis on a basin-by-basin basis.

Acknowledgments. The authors thank Christopher A. Davis, Robert Fovell, and two anonymous reviewers for their constructive comments about this research. Alan Brammer helped with access to reanalysis and TMPA datasets, and Kerry Emanuel provided code to calculate maximum potential intensity. High-computing resources and access to the RDA datasets was provided by NCAR's Computational Information Systems Laboratory via the Yellowstone supercomputing system (http://n2t.net/ark:/85065/d7wd3xhc). This work was funded by the National Science Foundation Graduate Research Fellowship Grant DGE 1060277 and the National Oceanic and Atmospheric Administration Grant NA14OAR4830172.

REFERENCES

Banzon, V. F., and R. W. Reynolds, 2013: Use of WindSat to extend a microwave-based daily optimum interpolation sea surface temperature time series. *J. Climate*, **26**, 2557–2562, doi:10.1175/JCLI-D-12-00628.1.

Bhatia, K. T., and D. S. Nolan, 2013: Relating the skill of tropical cyclone intensity forecasts to the synoptic environment. *Wea. Forecasting*, **28**, 961–980, doi:10.1175/WAF-D-12-00110.1.

Bister, M., and K. A. Emanuel, 2002: Low-frequency variability of tropical cyclone potential intensity 1. Interannual to interdecadal variability. *J. Geophys. Res.*, **107**, 4801, doi:10.1029/2001JD000776.

Black, M. L., J. F. Gamache, F. D. Marks, C. E. Samsury, and H. E. Willoughby, 2002: Eastern Pacific Hurricanes Jimena of 1991 and Olivia of 1994: The effect of vertical shear on structure and intensity. *Mon. Wea. Rev.*, **130**, 2291–2312, doi:10.1175/1520-0493(2002)130<2291:EPHJOA>2.0.CO;2.

Chen, H., and S. G. Gopalakrishnan, 2015: A study on the asymmetric rapid intensification of Hurricane Earl (2010) using the HWRF system. *J. Atmos. Sci.*, **72**, 531–550, doi:10.1175/JAS-D-14-0097.1.

Chen, S. S., J. A. Knaff, and F. D. Marks, 2006: Effects of vertical wind shear and storm motion on tropical cyclone rainfall asymmetries deduced from TRMM. *Mon. Wea. Rev.*, **134**, 3190–3208, doi:10.1175/MWR3245.1.

Computational and Information Systems Laboratory, 2012: Yellowstone: IBM iDataPlex System (University Community Computing). National Center for Atmospheric Research, Boulder, CO. [Available online at http://n2t.net/ark:/85065/d7wd3xhc.]

Corbosiero, K. L., and J. Molinari, 2002: The effects of vertical wind shear on the distribution of convection in tropical cyclones. *Mon. Wea. Rev.*, **130**, 2110–2123, doi:10.1175/1520-0493(2002)130<2110:TEOVWS>2.0.CO;2.

Davis, C., C. Snyder, and A. C. Didlake, 2008: A vortex-based perspective of eastern Pacific tropical cyclone formation. *Mon. Wea. Rev.*, **136**, 2461–2477, doi:10.1175/2007MWR2317.1.

Dee, D. P., and Coauthors, 2011: The ERA-Interim reanalysis: Configuration and performance of the data assimilation

system. *Quart. J. Roy. Meteor. Soc.*, **137**, 553–597, doi:10.1002/qj.828.

DeHart, J. C., R. A. Houze, and R. F. Rogers, 2014: Quadrant distribution of tropical cyclone inner-core kinematics in relation to environmental shear. *J. Atmos. Sci.*, **71**, 2713–2732, doi:10.1175/JAS-D-13-0298.1.

DeMaria, M., 1996: The effect of vertical shear on tropical cyclone intensity change. *J. Atmos. Sci.*, **53**, 2076–2088, doi:10.1175/1520-0469(1996)053<2076:TEOVSO>2.0.CO;2.

——, and J. Kaplan, 1994: A Statistical Hurricane Intensity Prediction Scheme (SHIPS) for the Atlantic basin. *Wea. Forecasting*, **9**, 209–220, doi:10.1175/1520-0434(1994)009<0209:ASHIPS>2.0.CO;2.

——, and ——, 1999: An updated Statistical Hurricane Intensity Prediction Scheme (SHIPS) for the Atlantic and Eastern North Pacific basins. *Wea. Forecasting*, **14**, 326–337, doi:10.1175/1520-0434(1999)014<0326:AUSHIP>2.0.CO;2.

ECMWF, 2009: ERA-Interim Project. Research Data Archive at the National Center for Atmospheric Research, Computational and Information Systems Laboratory, accessed 1 May 2016, doi:10.5065/D6CR5RD9.

Emanuel, K., C. DesAutels, C. Holloway, and R. Korty, 2004: Environmental control of tropical cyclone intensity. *J. Atmos. Sci.*, **61**, 843–858, doi:10.1175/1520-0469(2004)061<0843:ECOTCI>2.0.CO;2.

Finocchio, P. M., S. J. Majumdar, D. S. Nolan, and M. Iskandarani, 2016: Idealized tropical cyclone responses to the height and depth of environmental vertical wind shear. *Mon. Wea. Rev.*, **144**, 2155–2175, doi:10.1175/MWR-D-15-0320.1.

Galarneau, T. J., and C. A. Davis, 2013: Diagnosing forecast errors in tropical cyclone motion. *Mon. Wea. Rev.*, **141**, 405–430, doi:10.1175/MWR-D-12-00071.1.

Ge, X., T. Li, and M. Peng, 2013: Effects of vertical shears and midlevel dry air on tropical cyclone developments. *J. Atmos. Sci.*, **70**, 3859–3875, doi:10.1175/JAS-D-13-066.1.

Gray, W. M., 1968: Global view of the origin of tropical disturbances and storms. *Mon. Wea. Rev.*, **96**, 669–700, doi:10.1175/1520-0493(1968)096<0669:GVOTOO>2.0.CO;2.

Hence, D. A., and R. A. Houze, 2011: Vertical structure of hurricane eyewalls as seen by the TRMM Precipitation Radar. *J. Atmos. Sci.*, **68**, 1637–1652, doi:10.1175/2011JAS3578.1.

Hendricks, E. A., M. S. Peng, B. Fu, and T. Li, 2010: Quantifying environmental control on tropical cyclone intensity change. *Mon. Wea. Rev.*, **138**, 3243–3271, doi:10.1175/2010MWR3185.1.

Huffman, G. J., and Coauthors, 2007: The TRMM Multisatellite Precipitation Analysis (TMPA): Quasi-global, multiyear, combined-sensor precipitation estimates at fine scales. *J. Hydrometeor.*, **8**, 38–55, doi:10.1175/JHM560.1.

Jones, S. C., 1995: The evolution of vortices in vertical shear. I: Initially barotropic vortices. *Quart. J. Roy. Meteor. Soc.*, **121**, 821–851, doi:10.1002/qj.49712152406.

——, 2000: The evolution of vortices in vertical shear. II: Large-scale asymmetries. *Quart. J. Roy. Meteor. Soc.*, **126**, 3137–3159, doi:10.1002/qj.49712657008.

Kaplan, J., and M. DeMaria, 2003: Large-scale characteristics of rapidly intensifying tropical cyclones in the North Atlantic basin. *Wea. Forecasting*, **18**, 1093–1108, doi:10.1175/1520-0434(2003)018<1093:LCORIT>2.0.CO;2.

Knapp, K. R., M. C. Kruk, D. H. Levinson, H. J. Diamond, and C. J. Neumann, 2010: The International Best Track Archive for Climate Stewardship (IBTrACS). *Bull. Amer. Meteor. Soc.*, **91**, 363–376, doi:10.1175/2009BAMS2755.1.

Landsea, C. W., and J. L. Franklin, 2013: Atlantic hurricane database uncertainty and presentation of a new database format. *Mon. Wea. Rev.*, **141**, 3576–3592, doi:10.1175/MWR-D-12-00254.1.

MacQueen, J., 1967: Some methods for classification and analysis of multivariate observations. *Proceedings of the Fifth Berkeley Symposium on Mathematical Statistics and Probability, Volume 1: Statistics*, University of California Press, 281–297. [Available online at http://projecteuclid.org/euclid.bsmsp/1200512992.]

Merrill, R. T., 1988: Environmental influences on hurricane intensification. *J. Atmos. Sci.*, **45**, 1678–1687, doi:10.1175/1520-0469(1988)045<1678:EIOHI>2.0.CO;2.

Molinari, J., D. Vollaro, and K. L. Corbosiero, 2004: Tropical cyclone formation in a sheared environment: A case study. *J. Atmos. Sci.*, **61**, 2493–2509, doi:10.1175/JAS3291.1.

——, P. Dodge, D. Vollaro, K. L. Corbosiero, and F. Marks, 2006: Mesoscale aspects of the downshear reformation of a tropical cyclone. *J. Atmos. Sci.*, **63**, 341–354, doi:10.1175/JAS3591.1.

——, J. Frank, and D. Vollaro, 2013: Convective bursts, downdraft cooling, and boundary layer recovery in a sheared tropical storm. *Mon. Wea. Rev.*, **141**, 1048–1060, doi:10.1175/MWR-D-12-00135.1.

Munsell, E. B., F. Zhang, and D. P. Stern, 2013: Predictability and dynamics of a nonintensifying tropical storm: Erika (2009). *J. Atmos. Sci.*, **70**, 2505–2524, doi:10.1175/JAS-D-12-0243.1.

NCDC/NESDIS/NOAA, 2007: NOAA optimum interpolation 1/4 degree daily sea surface temperature analysis, version 2. Research Data Archive at the National Center for Atmospheric Research, Computational and Information Systems Laboratory, accessed 1 May 2016. [Available online at http://rda.ucar.edu/datasets/ds277.7/.]

Nguyen, L. T., and J. Molinari, 2012: Rapid intensification of a sheared, fast-moving hurricane over the Gulf Stream. *Mon. Wea. Rev.*, **140**, 3361–3378, doi:10.1175/MWR-D-11-00293.1.

——, and ——, 2015: Simulation of the downshear reformation of a tropical cyclone. *J. Atmos. Sci.*, **72**, 4529–4551, doi:10.1175/JAS-D-15-0036.1.

Onderlinde, M. J., and D. S. Nolan, 2014: Environmental helicity and its effects on development and intensification of tropical cyclones. *J. Atmos. Sci.*, **71**, 4308–4320, doi:10.1175/JAS-D-14-0085.1.

——, and ——, 2016: Tropical cyclone-relative environmental helicity and the pathways to intensification in shear. *J. Atmos. Sci.*, **73**, 869–890, doi:10.1175/JAS-D-15-0261.1.

Paterson, L. A., B. N. Hanstrum, N. E. Davidson, and H. C. Weber, 2005: Influence of environmental vertical wind shear on the intensity of hurricane-strength tropical cyclones in the Australian region. *Mon. Wea. Rev.*, **133**, 3644–3660, doi:10.1175/MWR3041.1.

Rappin, E. D., and D. S. Nolan, 2012: The effect of vertical shear orientation on tropical cyclogenesis. *Quart. J. Roy. Meteor. Soc.*, **138**, 1035–1054, doi:10.1002/qj.977.

Reasor, P. D., and M. D. Eastin, 2012: Rapidly intensifying Hurricane Guillermo (1997). Part II: Resilience in shear. *Mon. Wea. Rev.*, **140**, 425–444, doi:10.1175/MWR-D-11-00080.1.

——, and M. T. Montgomery, 2015: Evaluation of a heuristic model for tropical cyclone resilience. *J. Atmos. Sci.*, **72**, 1765–1782, doi:10.1175/JAS-D-14-0318.1.

——, ——, and L. D. Grasso, 2004: A new look at the problem of tropical cyclones in vertical shear flow: Vortex resiliency. *J. Atmos. Sci.*, **61**, 3–22, doi:10.1175/1520-0469(2004)061<0003:ANLATP>2.0.CO;2.

——, R. Rogers, and S. Lorsolo, 2013: Environmental flow impacts on tropical cyclone structure diagnosed from airborne Doppler radar composites. *Mon. Wea. Rev.*, **141**, 2949–2969, doi:10.1175/MWR-D-12-00334.1.

Reynolds, R. W., N. A. Rayner, T. M. Smith, D. C. Stokes, and W. Wang, 2002: An improved in situ and satellite SST analysis for climate. *J. Climate*, **15**, 1609–1625, doi:10.1175/1520-0442(2002)015<1609:AIISAS>2.0.CO;2.

——, T. M. Smith, C. Liu, D. B. Chelton, K. S. Casey, and M. G. Schlax, 2007: Daily high-resolution-blended analyses for sea surface temperature. *J. Climate*, **20**, 5473–5496, doi:10.1175/2007JCLI1824.1.

Riemer, M., and M. T. Montgomery, 2011: Simple kinematic models for the environmental interaction of tropical cyclones in vertical wind shear. *Atmos. Chem. Phys.*, **11**, 9395–9414, doi:10.5194/acp-11-9395-2011.

——, ——, and M. E. Nicholls, 2010: A New Paradigm for Intensity Modification of Tropical Cyclones: Thermodynamic Impact of Vertical Wind Shear on the Inflow Layer. *Atmos. Chem. Phys.*, **10** (7), 3163–3188, doi:10.5194/acp-10-3163-2010.

——, ——, and ——, 2013: Further examination of the thermodynamic modification of the inflow layer of tropical cyclones by vertical wind shear. *Atmos. Chem. Phys.*, **13**, 327–346, doi:10.5194/acp-13-327-2013.

Rios-Berrios, R., R. D. Torn, and C. A. Davis, 2016a: An ensemble approach to investigate tropical cyclone intensification in sheared environments. Part I: Katia (2011). *J. Atmos. Sci.*, **73**, 71–93, doi:10.1175/JAS-D-15-0052.1.

——, ——, and ——, 2016b: An ensemble approach to investigate tropical cyclone intensification in sheared environments. Part II: Ophelia (2011). *J. Atmos. Sci.*, **73**, 1555–1575, doi:10.1175/JAS-D-15-0245.1.

Ritchie, E. A., and W. M. Frank, 2007: Interactions between simulated tropical cyclones and an environment with a variable Coriolis parameter. *Mon. Wea. Rev.*, **135**, 1889–1905, doi:10.1175/MWR3359.1.

Rogers, R., P. Reasor, and S. Lorsolo, 2013: Airborne Doppler observations of the inner-core structural differences between intensifying and steady-state tropical cyclones. *Mon. Wea. Rev.*, **141**, 2970–2991, doi:10.1175/MWR-D-12-00357.1.

Rousseeuw, P. J., 1987: Silhouettes: A graphical aid to the interpretation and validation of cluster analysis. *J. Comput. Appl. Math.*, **20**, 53–65, doi:10.1016/0377-0427(87)90125-7.

Saha, S., and Coauthors, 2014: The NCEP Climate Forecast System version 2. *J. Climate*, **27**, 2185–2208, doi:10.1175/JCLI-D-12-00823.1.

——, and Coauthors, 2010: NCEP Climate Forecast System Reanalysis (CFSR) 6-hourly products, January 1979 to December 2010. Research Data Archive at the National Center for Atmospheric Research, Computational and Information Systems Laboratory, accessed 1 December 2015, doi:10.5065/D69K487J.

Schenkel, B. A., and R. E. Hart, 2012: An examination of tropical cyclone position, intensity, and intensity life cycle within atmospheric reanalysis datasets. *J. Climate*, **25**, 3453–3475, doi:10.1175/2011JCLI4208.1.

Shelton, K. L., and J. Molinari, 2009: Life of a six-hour hurricane. *Mon. Wea. Rev.*, **137**, 51–67, doi:10.1175/2008MWR2472.1.

Smith, R. K., G. Kilroy, and M. T. Montgomery, 2015: Why do model tropical cyclones intensify more rapidly at low latitudes? *J. Atmos. Sci.*, **72**, 1783–1804, doi:10.1175/JAS-D-14-0044.1.

Tang, B., and K. Emanuel, 2010: Midlevel ventilations constraint on tropical cyclone intensity. *J. Atmos. Sci.*, **67**, 1817–1830, doi:10.1175/2010JAS3318.1.

——, and ——, 2012: Sensitivity of tropical cyclone intensity to ventilation in an axisymmetric model. *J. Atmos. Sci.*, **69**, 2394–2413, doi:10.1175/JAS-D-11-0232.1.

Tao, D., and F. Zhang, 2014: Effect of environmental shear, sea-surface temperature, and ambient moisture on the formation and predictability of tropical cyclones: An ensemble-mean perspective. *J. Adv. Model. Earth Syst.*, **6**, 384–404, doi:10.1002/2014MS000314.

——, and ——, 2015: Effects of vertical wind shear on the predictability of tropical cyclones: Practical versus intrinsic limit. *J. Adv. Model. Earth Syst.*, **7**, 1534–1553, doi:10.1002/2015MS000474.

Torn, R. D., and C. Snyder, 2012: Uncertainty of tropical cyclone best-track information. *Wea. Forecasting*, **27**, 715–729, doi:10.1175/WAF-D-11-00085.1.

TRMM, 2011: TRMM/TMPA 3B42 TRMM and others rainfall estimate data V7. Goddard Space Flight Center Distributed Active Archive Center, accessed 15 June 2016. [Available online at https://mirador.gsfc.nasa.gov/collections/TRMM_3B42__007.shtml.]

Velden, C. S., and J. Sears, 2014: Computing deep-tropospheric vertical wind shear analyses for tropical cyclone applications: Does the methodology matter? *Wea. Forecasting*, **29**, 1169–1180, doi:10.1175/WAF-D-13-00147.1.

Wang, Y., Y. Rao, Z.-M. Tan, and D. Schnemann, 2015: A statistical analysis of the effects of vertical wind shear on tropical cyclone intensity change over the western North Pacific. *Mon. Wea. Rev.*, **143**, 3434–3453, doi:10.1175/MWR-D-15-0049.1.

Zeng, Z., Y. Wang, and L. Chen, 2010: A statistical analysis of vertical shear effect on tropical cyclone intensity change in the North Atlantic. *Geophys. Res. Lett.*, **37**, L02802, doi:10.1029/2009GL041788.

Zhang, F., and D. Tao, 2013: Effects of vertical wind shear on the predictability of tropical cyclones. *J. Atmos. Sci.*, **70**, 975–983, doi:10.1175/JAS-D-12-0133.1.

Zhou, W., 2015: The impact of vertical shear on the sensitivity of tropical cyclogenesis to environmental rotation and thermodynamic state. *J. Adv. Model. Earth Syst.*, **7**, 1872–1884, doi:10.1002/2015MS000543.